One Health 15 (2022) 100446

Contents lists available at ScienceDirect

One Health

journal homepage: www.elsevier.com/locate/onehlt

# Co-effects of global climatic dynamics and local climatic factors on scrub typhus in mainland China based on a nine-year time-frequency analysis

Junyu He [a,b,1], Yong Wang [c,1], Ping Liu [d,1], Wenwu Yin [e,1], Xianyu Wei [c], Hailong Sun [c], Yuanyong Xu [c], Shanshan Li [f], Ricardo J. Soares Magalhaes [g,h], Yuming Guo [f,**], Wenyi Zhang [c,*]

[a] Ocean College, Zhejiang University, Zhoushan, China
[b] Ocean Academy, Zhejiang University, Zhoushan, China
[c] Chinese PLA Center for Disease Control and Prevention, Beijing, China
[d] Department of General Practice, Chinese PLA General Hospital-Sixth Medical Center, Beijing, China
[e] Chinese Center for Disease Control and Prevention, Beijing, China
[f] Department of Epidemiology and Preventive Medicine, School of Public Health and Preventive Medicine, Monash University, Melbourne, Australia
[g] Spatial Epidemiology Laboratory, School of Veterinary Science, The University of Queensland, Brisbane, Australia
[h] Child Health Research Center, The University of Queensland, Brisbane, Australia

ARTICLE INFO

*Keywords:*
Scrub typhus
Clusters
Partial wavelet coherency
Climate
Wavelet power spectra

ABSTRACT

*Background:* Scrub Typhus (ST) is a rickettsial disease caused by *Orientia tsutsugamushi*. The number of ST cases has been increasing in China during the past decades, which attracts great concerns of the public health.
*Methods:* We obtained monthly documented ST cases greater than 54 cases in 434 counties of China during 2012–2020. Spatiotemporal wavelet analysis was conducted to identify the ST clusters with similar pattern of the temporal variation and explore the association between ST variation and El Niño and La Niña events. Wavelet coherency analysis and partial wavelet coherency analysis was employed to further explore the co-effects of global and local climatic factors on ST.
*Results:* Wavelet cluster analysis detected seven clusters in China, three of which are mainly distributed in Eastern China, while the other four clusters are located in the Southern China. Among the seven clusters, summer and autumn-winter peak of ST are the two main outbreak periods; while stable and fluctuated periodic feature of ST series was found at 12-month and 4-(or 6-) month according to the wavelet power spectra. Similarly, the three-character bands were also found in the associations between ST and El Niño and La Niña events, among which the 12-month period band showed weakest climate-ST association and the other two bands owned stronger association, indicating that the global climate dynamics may have short-term effects on the ST variations. Meanwhile, 12-month period band with strong association was found between the four local climatic factors (precipitation, pressure, relative humidity and temperature) and the ST variations. Further, partial wavelet coherency analysis suggested that global climatic dynamics dominate annual ST variations, while local climatic factors dominate the small periods.
*Conclusion:* The ST variations are not directly attributable to the change in large-scale climate. The existence of these plausible climatic determinants stimulates the interests for more insights into the epidemiology of ST, which is important for devising prevention and early warning strategies.

*Abbreviations:* ST, Scrub Typhus; MEI, multivariate El Niño Southern Oscillation index; ENSO, El Niño Southern Oscillation; SST, Sea surface temperature; NSI, Niño 3.4 SST index.

* Correspondence to: W Zhang, Chinese PLA Center for Disease Control and Prevention, 20 Dong-Da Street, Fengtai District, Beijing 100071, China.
** Correspondence to: Y Guo, School of Public Health and Preventive Medicine, Monash University, Level 2, 553 St Kilda Road, Melbourne, VIC 3004, Australia.
*E-mail addresses:* yuming.guo@monash.edu (Y. Guo), zhangwenyi@bmi.ac.cn (W. Zhang).
[1] These authors contributed equally to this work.

https://doi.org/10.1016/j.onehlt.2022.100446
Received 20 June 2022; Received in revised form 4 September 2022; Accepted 11 October 2022
Available online 13 October 2022

## 1. Introduction

Scrub Typhus (ST) is a rickettsial disease caused by *Orientia tsutsugamushi*, which is transmitted to humans by the bite of larvae of trombiculid mites. The most common symptoms include high fever, headache, acute hearing loss, pneumonitis [1]. As a mite-borne disease, the main domestic animals carrying the rickettsia are *Apodemus agraius*, *Micromys minutus*, *Rattus norvegicus* [2,3]. ST has become a major public health problem due to its large distribution in Asia [4]. The number of ST cases has been sharply increased since 2006 in China [5,6]. Furthermore, female had a higher incidence than male, and farmers had a higher incidence than non-farmers [5,6]. Therefore, it is of great importance to study the distribution characteristics of ST for better monitoring, surveillance and prevention purposes.

Summer ST and Autumn-Winter ST were found to be the two main temporal characteristics in mainland China for the Southern provinces and Northern provinces, respectively [5,7,8]. Many hotspots and high-risk space-time clusters were identified in the south and southwest of China by using local indicators of spatial association and Kulldorff's space-time scan statistics [9,10]. Although the main clusters of ST in China were detected in the above studies, only intuitive ST cases or incidences series were put into considerations; thus, it is worthy to utilize the inherent variation of ST series to explore the clusters with the help of time-frequency technique.

Wavelet analysis has been proven to be a powerful tool in handling non-stationary time series [11]. Compared to the Fourier transformation technique, wavelet analysis can not only explore the temporal pattern of the time series in frequency domain, but also in time domain. For instance, the recurrence feature of measles, chicken pox, rubella and whooping cough were studied by using the wavelet power spectra [12]. Using the wavelet power spectra, previous studies found that an annual cycle of Dengue fever was detected in all provinces of southern Vietnam with substantial heterogeneity [13,14]. In order to delimit the regions with similar variation pattern, wavelet cluster analysis was developed by comparing the wavelet power spectrum at each region or location [15], and it has been applied to explore the cluster feature of pneumonia hospitalizations in Netherland, tuna and billfish time series of catch and catch per unit efforts in the Eastern Canary Coastal province on the west African coast [16,17]. However, the wavelet cluster analysis of ST time series in China is still lacking. With these defined clusters, more detailed information on the transmission patterns of ST within various clusters can be dug out for comparison purposes.

During the last decades, the climatic impacts on the evolution of ST is also a hot topic because the variation of climatic factors will influence the survival of rodents and the chiggers [8]. The association was found between temperature, snowfall and maximum depth of snow cover with ST cases by using negative binomial regression model [18]. One previous study combined negative binominal regression model with a distributed lag non-linear model (DLNM) to investigate the non-linear effect of different humidity types on ST occurrence, and they found W-shaped non-linear association for all humidity types [4]. Another study from China demonstrated that the relative humidity, rainfall, diurnal temperature range, multivariate El Niño Southern Oscillation index (MEI) and rodent density were associated with the incidence of ST by using a time-series Poisson regression model with DLNM [19]. Most of the ST studies focus on the direct impact on the risk of ST without the inherent co-variation analysis between the predictors and ST. Given that the wavelet coherency analysis technique was able to quantitatively measure the strength between two related time series in many studies [20–24], the wavelet coherency analysis between ST and climatic variables is worthy to be conducted and will benefit the local disease monitoring and control purposes.

In view of the above considerations, the objectives of this study are to investigate the periodic characteristic of ST in China, and define the wavelet clusters of ST variations and the temporal pattern of each cluster, and explore coupling effects of El Niño and La Niña events and local climatic factors on ST using wavelet analysis technique.

## 2. Materials and methods

### 2.1. Study area and data collection

Monthly ST cases at 2853 districts, counties or county-level cities were collected in the mainland China during the study period 2012–2020 from the China Information System for Disease Control and Prevention. The criteria for a confirmed ST case included epidemiological exposure patient histories (travel to an epidemic area and contact with chiggers or rodents within 3 weeks before the onset of illness), clinical manifestations (for example, skin rash, lymphadenopathy, high fever, and eschar or ulcers), and also positivity for at least one of the laboratory diagnostic criteria/tests: isolation of *O. tsutsugamushi* from clinical specimens, or detection of *O. tsutsugamushi* by polymerase chain reaction (PCR) in clinical specimens, or a 4-fold or greater rise in serum IgG antibody titers between acute and convalescent sera by using indirect immunofluorescence antibody assay (IFA) [6]. Among all counties, there are 1463, 956 and 434 counties that documented zero, less than or equal to 54 cases, and larger than 54 cases, respectively. Only the counties with reported ST cases larger than 54 were considered for wavelet analysis. On the other hand, two global climatic oscillation indices were collected for exploring its association with ST variation: Niño 3.4 SST index (NSI), defining El Niño and La Niña events, was downloaded from https://psl.noaa.gov/gcos_wgsp/Timeseries/Data/nino34.long.anom.data; meanwhile, the multivariate El Niño Southern Oscillation index (MEI), which can be used to diagnose ENSO phenomena, was downloaded from https://psl.noaa.gov/enso/mei/data/meiv2.data. The local climatic factors, including precipitation, pressure, relative humidity and temperature, were collected from the China Meteorological Administration (http://www.cma.gov.cn/).

### 2.2. Wavelet cluster analysis

To obtain spatial and temporal ST clusters with similar temporal variation, three stages were implemented as following. (a) The ST series at each of the 434 counties was separately wavelet transformed by using Eq. (1),

$$W(\tau,\alpha)=\frac{1}{\sqrt{\alpha}}\int_{-\infty}^{+\infty} ST(t)\psi^{*}\left(\frac{t-\tau}{\alpha}\right)dt \tag{1}$$

where $\psi(\bullet)$ is the Morlet wavelet, $\alpha$ and $\tau$ represent the scale factor and time shift, respectively. (b) Thus, the wavelet power spectrum (WPS) at each county can be calculated by Eq. (2), which can be used to detect the variability of ST series in both time and frequency domains.

$$WPS(\tau,\alpha)=|W(\tau,\alpha)|^{2} \tag{2}$$

(c) Maximum covariance analysis (MCA), also called singular value decomposition, was employed to compare the similarity between the pairs of the 434 wavelet power spectra as following: the $k^{\text{th}}$ leading patterns $L^{k}$ of the paired *WPS* were calculated by projecting the WPS onto its perspective singular vectors as Eq. (3) shows,

$$\begin{cases} L_i^k(t)=\int_{f=1}^{F}\boldsymbol{U}^k\times WPS_i(f,t) \\ L_j^k(t)=\int_{f=1}^{F}\boldsymbol{V}^k\times WPS_j(f,t) \end{cases} \tag{3a-3b}$$

where the columns of matrix $\boldsymbol{U}$ contain the singular vector of $WPS_i$, while the rows of matrix $\boldsymbol{V}$ contain the singular vectors of $WPS_j$, $F$ is the maximum frequency within the two spectra; and distance ($DT$) between the two spectra can be obtained by Eq. (4), as follows:

$$\begin{cases} D\left(L_i^k, L_j^k\right) = \sum_{t=1}^{n-1} arctan\left[\left|\left(L_i^k(t) - L_j^k(t)\right) - \left(L_i^k(t+1) - L_j^k(t+1)\right)\right|\right] \\ DT(i,j) = \dfrac{\sum_{k=1}^{K} w_k \times \left[D\left(L_i^k, L_j^k\right) + D\left(\boldsymbol{U}_i^k, \boldsymbol{V}_j^k\right)\right]}{\sum_{k=1}^{K} w_k} \end{cases} \quad (4a\text{-}4b)$$

where $n$ is the length of the singular vectors, and $w_k$ is the weights equaling to the amount of covariance explained by each axis. More detailed information can be found in the literature [15].

With the procedure mentioned above, a number of spatial and temporal ST clusters can be obtained, and the averaged *WPS* of each cluster was calculated for comparison purpose, as well as the temporal variation characteristics of ST. The wavelet analysis was implemented in R software.

### 2.3. Wavelet coherency analysis for association between ST and El Niño and La Niña events

Wavelet coherency analysis was employed to explore the association between the global climate dynamics (depicted by MEI or NSI) and the ST cases at each of the considered 434 counties, separately, i.e., through wavelet transformation (Eq. 1) and cross-wavelet transformation (Eq. 5a), the wavelet coherency was derived by normalizing the cross-wavelet with the spectrum of each series (Eq. 5b), as following:

$$\begin{cases} W_{ENSO-ST} = W_{ENSO} W_{ST}^* \\ C_{ENSO-ST}(\tau,\alpha) = \dfrac{\| \langle W_{ENSO-ST}(\tau,\alpha) \rangle \|}{\| \langle W_{ENSO}(\tau,\alpha) \rangle \|^{1/2} \| \langle W_{ST}(\tau,\alpha) \rangle \|^{1/2}} \end{cases} \quad (5a\text{-}5b)$$

where $W_{ENSO}$ and $W_{ST}$ represent the wavelet transformed series of ENSO index (MEI or NSI) and ST cases, respectively. *, <> and || || denote the complex conjugate, smoothing and modulus operator, respectively. The wavelet coherency $C_{ENSO-ST}(\tau,\alpha)$ was used to quantitatively measure the strength of the co-variation between the two series. The averaged wavelet coherency spectra were calculated at each cluster for comparison purposes and the temporal variation of the character periods were also discussed. In the present study, wavelet analysis was conducted by the "biwavelet" package in R software (version 4.0.5), and the maps were plotted by QGIS software (version 3.18.2).

### 2.4. Partial wavelet coherency analysis for association between ST and El Niño and La Niña events by removing the effects of local climatic factors

Given the ST variation can be influenced by both global climatic factor (El Niño and La Niña events) and local climatic factors, the partial wavelet coherency is appropriate to detect the impacts of global factors that removing the effects of local climatic factors by using Eq. (6).

$$C(ST, ENSO, x) = \frac{\left|C_{ST-ENSO} - C_{ST-x} \bullet C_{ST-ENSO}^*\right|}{[1 - C_{ST-x}][1 - C_{ENSO-x}]} \quad (6)$$

where $x$ represents the local climatic factors, such as precipitation, pressure, relative humidity and temperature. Through comparing the values of partial wavelet coherency and the wavelet coherency values, the effects of local climatic factors can be further detected. For example, if $C_{ENSO-ST} > C(ST, ENSO, x)$ at specific a frequency and temporal span, it explains the impacts of local climatic factor $x$ on ST cannot be ignored; in contrary, the impacts of the local climatic factor on ST can be ignored.

## 3. Results

### 3.1. Wavelet clusters of ST

By comparing the wavelet power spectra of ST series obtained at 434 counties, the cluster tree with seven simplified clusters was finally yielded as shown in Fig. 1a; the complete cluster tree can be found in Appendix (Fig. A1). It was found that clusters 1–3 and clusters 4–7 are separately distributed in the eastern and southern China (Fig. 1b). More specifically, the number of counties belongs to each of clusters 1–7 is 26, 46, 43, 99, 19, 80, 121, respectively. The wavelet power spectrum of ST series in China shows three main periods across the entire study period, i.e., 4-month, 6-month and 12-month periods, among which the 12-month period displays the strongest annual periodicity as very high wavelet power value was detected with yellow-red color shown in Fig. 2a. Fig. 2b-2h shows the averaged wavelet power spectra of ST series in the counties in each of the seven cluster, respectively. The averaged spectra of clusters 2 and 4 were very similar to the spectrum of the entire China. For clusters 1 and 4, the global averaged wavelet power values at 4- or 6-month period is at the same order of magnitude; while for clusters 1, 2, 4 and 6, high continuous wavelet power values are detected at periodic temporal instants, i.e., the vertical ribbon-like regions from 1- to 6-month period. For clusters 5 and 7, the periodicity characteristics of 12-month band were rather strong since 2018. Fig. 2i and Fig. A2 represent the wavelet power spectrum of NSI and MEI, respectively. The two spectra of ENSO indices are rather similar, displaying high wavelet power values at 18-month period from 2015 to 2017, which is different from the wavelet power spectra of ST. Annual periodic characteristics of the four local climatic factors were detected by the wavelet power spectra (Fig. A3).

The wavelet spectra of scrub typhus time series at each of 434 countries with scrub typhus cases larger than 54 were compared and a dissimilarity matrix was produced for generating wavelet clusters. The simplified cluster tree and spatial distribution of each cluster were shown in (a) and (b), respectively. In the subfigure (b), "no data" represents the counties of Taiwan that we didn't collect and analyze the scrub typhus data; "no cases" and "≤54 cases" represent the counties of mainland China that no scrub typhus cases and less than 54 cases were reported during 2012–2020, which were not considered in the current study; while the other items in the legend represents that the counties belong to the corresponding cluster.

Through extracting the wavelet power values at 4-, 6-, 12-month periods, the log-transformed wavelet power values of the seven clusters across the temporal dimension are shown in Fig. A4. In general, an increasing trend for various clusters and periods can be found. Specifically, the wavelet power values fluctuate a lot and exhibit periodic characteristics at 4-month period (Fig. A4a) comparing to the other two periods. The patterns for the seven clusters at 12-month period (Fig. A4c) are much smoother than the other two periods. On the other hand, the order of power values for the seven clusters are similar in the three subfigures. For example, the power values of cluster 1 are the highest among the seven clusters; while cluster 7 and cluster 6 experience the lowest value before 2017 and after 2017, respectively; specifically, the V-shape temporal pattern of power values for cluster 5 is rather different from the other six clusters.

### 3.2. Temporal patterns of ST

After defining the seven clusters of ST in China, the total number of ST cases at each year and month during the 2012–2020 were shown in Fig. 3a-3b. Several features can be summarized: (a) among the seven clusters, cluster 4 (with 99 counties) occupies the largest number of ST cases with apparent increasing trend, while cluster 7 (with 121 counties) owns the second largest number; (b) the annual ST cases of cluster 5 (with 19 counties) increase rapidly since 2018; (c) the ST cases in clusters 1, 2, 3 and 5 (with 26, 46, 43 and 19 counties, respectively) experience an increasing period from 2012 to 2016, and then become stable until 2020. According to the monthly ST curves shown in Fig. 3b, three types of patterns can be detected: (a) the ST cases peak in autumn-winter season (October or November) for clusters 1, 2 and 3; (b) two peaks at June and November can be found in cluster 5; (c) the ST cases

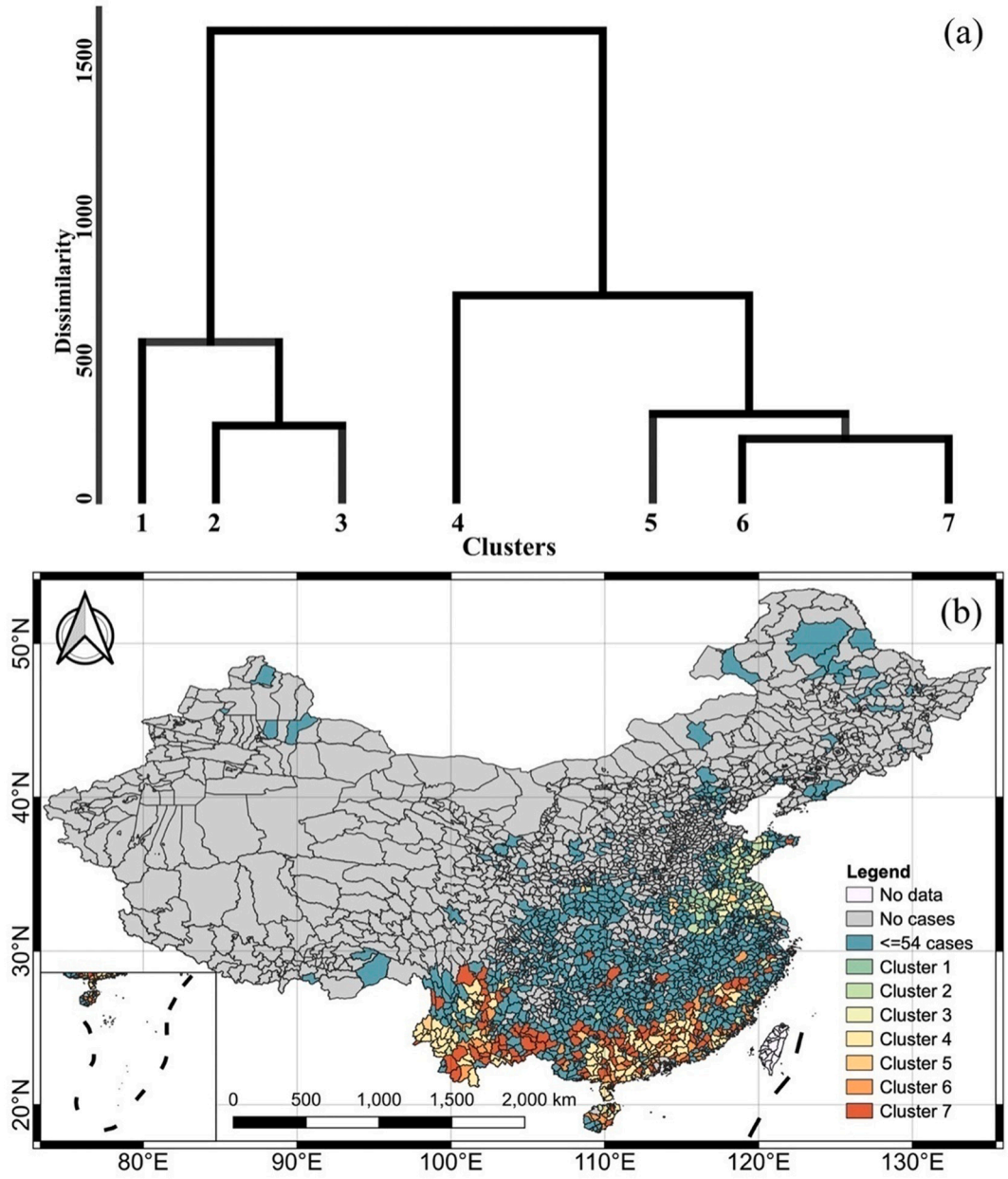


**Fig. 1.** Wavelet cluster analysis results of scrub typhus time series at 434 counties in mainland China.

will outbreak at summer season (July or August) in the counties of cluster 4, 6 and 7.

### 3.3. *Wavelet coherency analysis*

The averaged wavelet coherency spectra between ST cases and NSI are shown in Fig. A5. In general, high and low coherency values appear alternately at 2- to 4-month period band; the cluster 5 visualized differently due to the high coherency values across 2–5-month period bands at the early stage of 2012. Some high values can be found at 6-month band across the period from 2013 to 2014 and 2018 to 2019; however, the values at 12-month band are relatively small. By comparing the wavelet coherency spectra among various clusters, the spectra of cluster 1, 2 and 3 are rather similar, while the spectra of cluster 4, 6 and 7 are similar but with various magnitude at specific time-frequency regions.

Selecting the 4-, 6- and 12-month period bands, the temporal series of the wavelet coherency values for each cluster are shown in Fig. A6. The coherency values fluctuate at a larger amplitude for 4-month and 6-month periods than for the 12-month period. The variation of coherency values of cluster 5 are rather different from the other six clusters; clusters 1–3 exhibit similar temporal pattern during the entire study period; while coherency values of clusters 4, 6 and 7 co-varies a lot in most parts of the entire temporal spans. Specifically, the three kinds of variation pattern differ distinct at 4-month period, while the patterns become more similar at 6- and 12-month period bands, except the cluster 5. Lastly, lowest coherency values were detected at 12-month period band among the three bands. Additionally, the phase difference for clusters 6 and 7 shows more stable than the other clusters (Fig. A7), while the phase difference for 12-month period shows less fluctuation than 4- and 6-month periods.

Similar findings can also be concluded for the wavelet coherency spectra between ST and MEI, together with the temporal series of the wavelet coherency values at 4-, 6- and 12-month period shown in Figs. A8 and A9. However, the coherency values of clusters 1, 2, and 3 are larger than the values of clusters 4, 6, and 7 during most of the

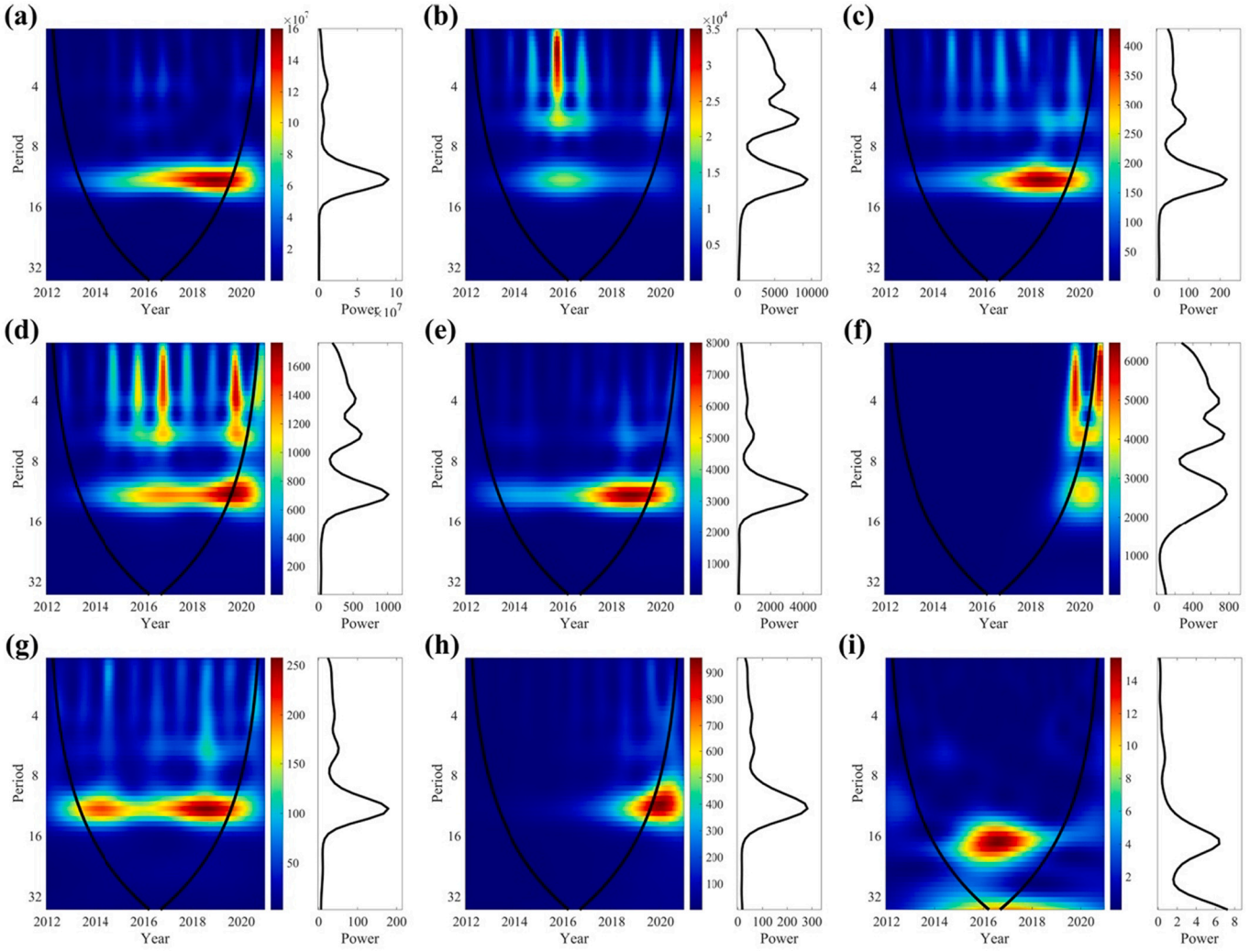


**Fig. 2.** Wavelet power spectra of the Scrub typhus cases for (a) the entire mainland China and (b-h) the seven clusters, and (i) the Niño 3.4 SST index. The left part of each subfigure represents the wavelet power spectrum at time-frequency domain, while the right part represents the global averaged power values at corresponding frequency domain. Black lines in the spectra represent the significant areas at the 5% level, and the color from blue to red display the low to high wavelet power values, indicating the cyclic strength. (For interpretation of the references to color in this figure legend, the reader is referred to the web version of this article.)

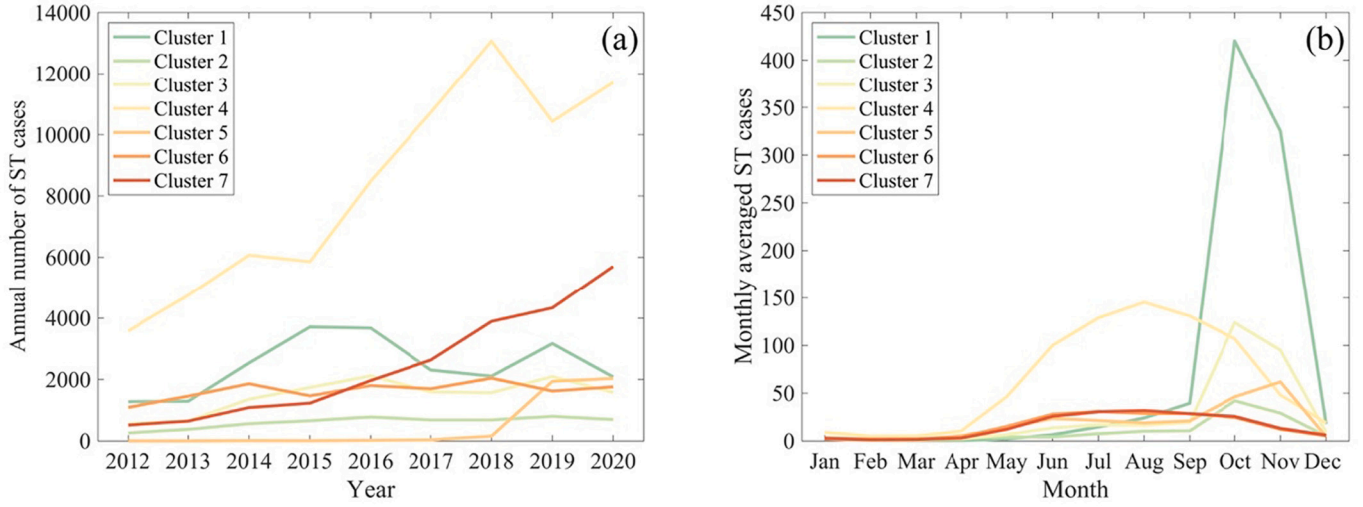


**Fig. 3.** Temporal pattern of Scrub typhus cases for the seven clusters at (a) annual scale and (b) monthly scale. The curves in the two subfigures represent the variations of scrub typhus cases by averaging the annual or monthly scrub typhus cases at the counties of each cluster.

studying period, which is opposite to the findings between ST and NSI. On the other hand, the wavelet coherency spectra between ST and the four local climatic factors (i.e., precipitation, pressure, relative humidity and temperature) shows 12-month co-variation characteristics for the 7 clusters except for cluster 5 (Fig. A10-A13). Meanwhile, the phase difference shows rather stable characteristics at 12-month period for the four variables (Fig. A7).

Through averaging the coherency values across the entire study period, the mean coherency value between ST and NSI (or MEI) at each of the considered counties were shown in Fig. 4 (or Fig. A14). The mean coherency values are rather different for the two associations (i.e., ST-NSI, or ST-MEI): similar mean coherency values were found at both eastern China and southern China for ST-NSI at 4-, 6-, and 12-month period bands, but the mean coherency values of ST-MEI at eastern China are smaller than the values at southern China at 4- and 6-month period bands. Moreover, it is obvious that the high mean coherency values between ST and NSI occupy larger proportion of the counties for each of the seven clusters at 6-month period band than at 4-month period band; while the 12-month period band shows the largest proportion with low mean coherency values (Fig. A15). On the other hand, the proportion of counties with high mean coherency values between ST and MEI at 4-month period band is larger than the corresponding proportion at 6-month period band for the seven clusters except cluster 5; similarly, larger proportion of the counties with low mean coherency values can be found at 12-month period band (Fig. A15). Various coherency strength between ST and the four local climatic factors at different counties can be found in Fig. A16.

### 3.4. Partial wavelet coherency analysis

Through comparing the wavelet coherency spectra and partial wavelet coherency spectra, the coupling effects of El Niño/La Niña events and local climatic factors on Scrub typhus can be further investigated. As is shown in Figs. 5 and 6, high positive values of the differences between wavelet coherency spectra and partial wavelet coherency spectra related to Niño 3.4 SST index can be found at low period domain, indicating that the local climatic factors show more dominance on the ST variation than the Niño 3.4 SST index. Specifically, local climatic factors display stronger effects on ST variation for clusters 6 and 7 than the other five clusters in terms of the curves in Fig. 6. Regarding the 12-month period, negative values of the differences were detected, suggesting that the local climatic factors are not that important for influencing the ST variations by considering the coupling effects of global and local factors; on the other hands, the local climatic factors at 12-month period may not closely related to the El Niño/La Niña events. Similar findings can be also concluded for the multivariate El Niño Southern Oscillation index (Figs. A17 and A18).

## 4. Discussions

### 4.1. Moran effects on the determination of ST clusters

Moran effects were proposed as a phenomenon that spatially synchronous variations of environment can lead to synchronous variations in the species abundance [25,26], which is also found in the present study in two-fold: (a) although the ST series varies with each other at different counties, the temporal variation pattern can be summarized to follows six clusters by wavelet cluster analysis, each of which are located in the neighbor regions (Fig. 1).The clustered distribution of summer ST or autumn ST is an important reason for strengthening the Moran effect [27]. Noteworthy, the Moran effects discovered in the present study rely on the ST variation in a space-time-frequency domain in terms of the wavelet power spectra (Fig. 2), which is rather different compared to the traditional purely spatial point of view on Moran effects [25,28,29]. (b) The wavelet coherency analysis, describing the inherent association between ST cases and global climate dynamics, also yields long-term strong climatic Moran effects according to the wavelet coherency spectra (Figs. A5 and A8).The above two kinds of Moran effects may due to the fact that the global climate dynamics and local environmental or geographical factors (such as distance to cropland, elevation, precipitation, etc.) synchronously varies at these neighbor regions [29], which also lead to similar relative risk of ST for human [30,31]. In summary, the ST series owns Moran effect in a space-time-frequency domain with the synchronous variation of the environmental factors, leading to various ST clusters.

### 4.2. Temporal characteristics of ST clusters

A central outcome of the current study is the successful determination of the seven ST clusters in the 434 considered counties by wavelet analysis. Our results showed that the ST variation are strongly clustered in space-time-frequency domain. To the best of our knowledge, this is one of the earliest studies to characterize the cluster feature of ST variation in China. Specifically, the 12-month period was found to be continuously strong during the study period, especially during the second half period (Fig. 2), which is similar to the findings in [19]. It suggested that the ST variation may be closely linked to the annually variation of climate [32]. In addition, 4- and 6-month periods were also detected as the temporal pattern of ST at a smaller scale, which can be regarded as the character period of its own variation; Wu et al. [9] also detected the 6-month as a seasonal trends of ST variation in Mainland China. However, the wavelet power values at these two small scales were fluctuated during the entire study period (Fig. A4), which may be attributed to the fact that the ST will outbreak in one or two months in one calendar year, while the number of ST cases were rather small or even zero at the other months. Regarding the temporal trends of the ST clusters, the summer ST peaks or autumn-winter ST peaks are the two main features, which has also been reported in several literatures with more historical ST data [5,9,27]. In other words, these features don't change with time and may be the inherent genetic pattern of ST, such as the aggregation of hosts for mitigating the climatic impacts and the population increments in the early winter period [33,34].The differences between the summer type and the autumn-winter type includes the geographical distribution, key reservoir hosts, key vector chigger mites, etc. [35,36].

### 4.3. The impacts of environmental factors on the ST variation

On one hand, the variation of ST cases that might display both short- and long-term oscillations due to the residents of virus hosts and the interactions between the rodents and human beings [19]. According to the literatures, the ST cases is no longer a rural disease, but also become an urban disease with significant increasing trend, due to the appropriate living conditions for vectors and small rodents in urban parks [37–41]. Besides, the connection between rural and urban areas becomes much closer with the development of the society and economics, making the ST variation more complex, i.e., such as the frequency of trade and travel for human beings and the modern agriculture practices [31]. There is another study confirmed that the gross domestic product, representing the level of urbanization, contributed most for the boost regression tree model in Qingdao City, China [42]. In other words, the human factors have been becoming another significant impact factor on ST infections, which makes the characteristics not that stable with high wavelet power values in Fig. 2 during the entire study periods, especially for the small scale of period.

On the other hand, the population of rodents is not isolated and is magnificently affected by the ecosystem that is controlled by climatic variations. Global climate dynamics (ENSO) was closely linked to the increment of the rodents' population through a complex way [43–45], further affecting the transmission of the zoonoses disease, such as ST, cholera, malaria, hantavirus pulmonary syndrome, hemorrhagic fever with renal syndrome, plague [46–48]. For example, a trophic cascade

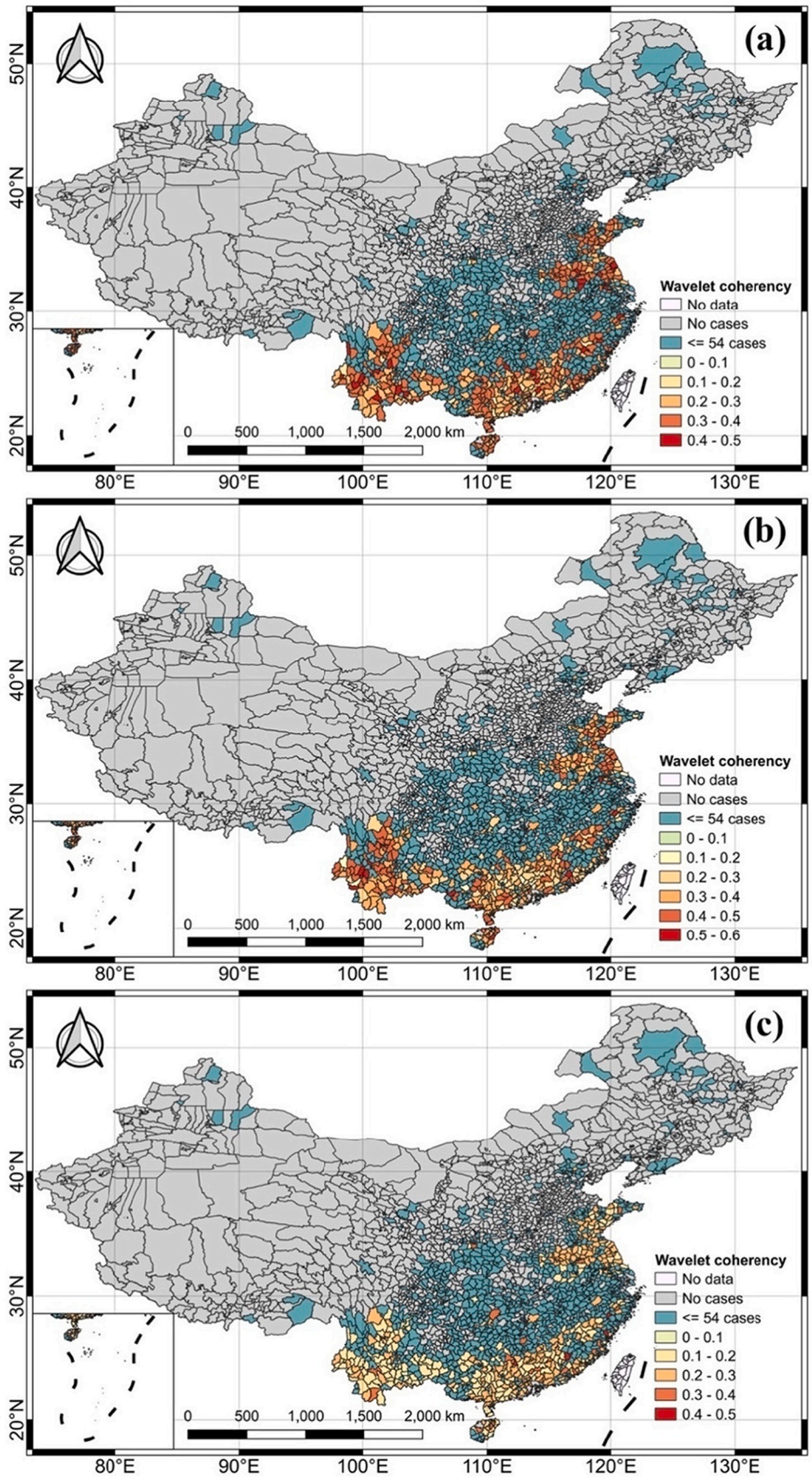


**Fig. 4.** Maps of the averaged association strength between the Scrub typhus cases and Niño 3.4 SST index during the period 2012–2020 at (a) 4-month period, (b) 6-month period, (c) 12-month period. The averaged association strength (i.e., the wavelet coherency values) at each county was calculated by averaging the values at 4-. 6- or 12-month period band (y-axis) of the wavelet coherency spectra during 2012–2020. "No cases" and "≤54 cases" represent the counties of mainland China that no scrub typhus cases and less than 54 cases were reported during 2012–2020, which were not considered in the current study.

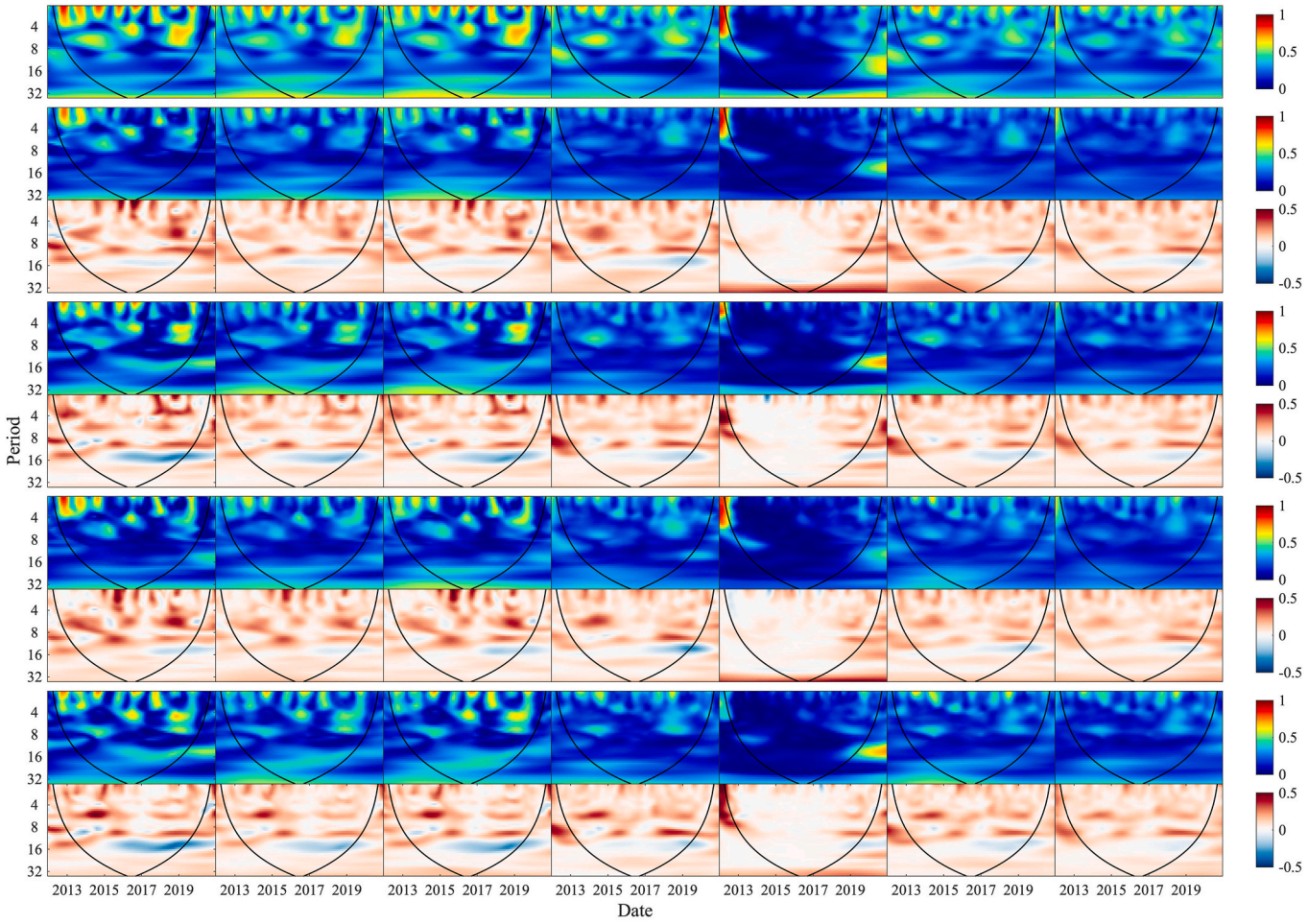


**Fig. 5.** Wavelet coherency spectra and partial wavelet coherency spectra. The subplots in Row 1 represent the wavelet coherency spectra between Niño 3.4 SST index and Scrub Typhus cases for each of the seven clusters; the subplots in Row 2, 4, 6, 8 represent the partial wavelet coherency spectra between Niño 3.4 SST index and Scrub Typhus cases excluding the effects of precipitation, pressure, relative humidity and temperature, respectively, for each of the seven clusters; the subplots in Row 3, 5, 7, 9, represents the spectra difference between the spectra in Row 1 and Row 2, 4, 6, 8, respectively. The color bar in each row represents the values of wavelet coherency or partial wavelet coherency. For the partial wavelet coherency spectra, negative values represent that the value of the wavelet coherency spectra at specific time instant (x-axis) and frequency (y-axis) is smaller than the value of partial wavelet coherency spectra at the same time instant and frequency, while the positive values are the opposite situation.

between ENSO and vector-borne disease was detected as follows: global climate dynamics partly dominate the local climatic factors (such as temperature, precipitation and relative humidity) [49–51]; while the local geographical factors (such as land cover and land use types) will also make great contribution for the impacts of global climate dynamics on local climate situations [22], i.e., each geographic area will display particular climate dynamics. These local climatic factors further affect the living environment of rodents and the primary food production, which favor the growth of rodents; specifically, warming environment favor the growth of vector larvae, and the relative humidity was found to be the key factor for the re-generation of the rodents [8,52]. As a result, the probability of the contact between rodents and human increases accordingly. Therefore, ENSO influence ST infection in an indirect way. Wei et al., [19] also detected the impact of ENSO on ST, but with 5-month temporal lag effects, and it is in line with results of the present study, i.e., the wavelet coherency values are not very high and stable during the study period (Figs. A5 and A8).

### 4.4. Contribution to public health

The methodology used in the current study gives a way for the public health authorities to understand either global climatic dynamics or local climatic factors give more contribution to the ST variation at specific periods; and they can give more attention to the significant factors. Moreover, the cluster analysis identifies the similar temporal patterns of ST for various counties, and the public health authorities of a county will benefit by any effective HFRS control measures previously implemented in other counties within the same clusters.

### 4.5. Limitations and future work

According to the wavelet coherency analysis, the association between the ST case and global climate dynamic was high at small temporal scale, indicating that the ST variation may be affected by some other local factors. Several historical literatures reported that temperature, precipitation, humidity, and sunshine duration was closely related to the variation of ST cases [8,27,52,53]. Therefore, it is worthy to explore the association between ST cases and local climatic conditions at a national scale by using wavelet coherency analysis, distributed lag nonlinear models or ecological niche model in the future [3,19,27]. In addition, given that cluster analysis can be implemented by wavelet analysis, other time-frequency analysis methodology (such as Hilbert-Huang analysis with ensemble empirical mode decomposition) can be further considered for exploring the temporal variation of ST series [24]. Last but not least, socioeconomic factors are also related to ST cases; for example, urbanization and higher school enrollment rates are negative

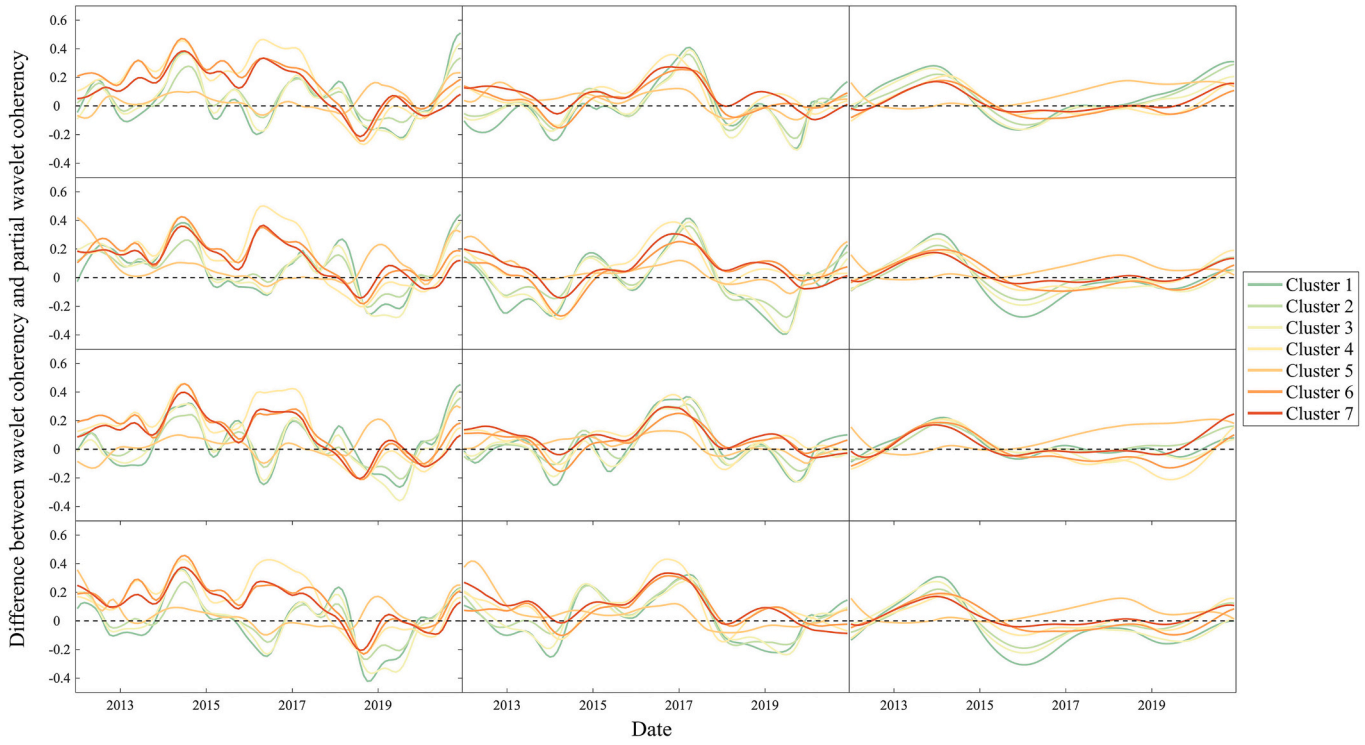


**Fig. 6.** Spectra difference between wavelet coherency spectra for Niño 3.4 SST index-Scrub Typhus cases association and partial wavelet coherency spectra for the association excluding the effects of four meteorological variables. The subplots from Row 1 to 4 respectively represent the spectra difference for precipitation, pressure, relative humidity, temperature; while the subplots from Column 1 to 3 represent the spectra difference at 4, 6, and 12-month period, respectively.

related to ST cases, while the farmers have more probability to be infected with ST [31,54,55]. Therefore, future work should also include the socioeconomic factors for detecting the potential impact factors of ST.

## 5. Conclusion

This study explored the ST dynamics at 434 counties of China by wavelet analysis, and seven clusters with similar temporal patterns in space-time-frequency domain. Summer and autumn-winter outbreak of ST was detected within various clusters. The wavelet power spectra summarized multi-scale mode of oscillation with significant periods at 4-, 6- and 12-month. Understanding the interactions between the global climate dynamics and ST variation is a key question for disease monitoring and management. To this end, wavelet coherency analysis was conducted, and the results reported moderate non-stationary association between global climate dynamics (using NSI and MEI as proxy) and ST variation for multi-scale cycle. On the other hand, strong association between local climatic factors (including precipitation, pressure, relative humidity, temperature) were detected at 12-month period. By comparison, local climatic factors show more dominance on ST variation at small periods, while the global climatic climate dynamics shows larger impacts on ST variation at annual period. This existence of these plausible climatic determinants stimulates the interests for more insights into the epidemiology of ST, which is important for devising prevention and early warning strategies.

## Ethics approval and consent to participate

The present study was approved by (a) the Chinese Center for Disease Control and Prevention, and (b) Chinese PLA Center for Disease Control and Prevention. All ST data were anonymously analyzed.

## Consent for publication

Not applicable.

## Availability of data and materials

Patient data are protected by the China CDC and are unsuitable for public sharing. The ST data is not allowed to be publicly shared due to local infection disease law. Interested parties can apply for the data by contacting the Data-center of China Public Health Science (http://www.phsciencedata.cn/Share/ky_sjml.jsp?id=59761d3e-ca3c-4c65-a6a567be1d2fb692) or email data@chinacdc.cn.

## Competing interests

The authors declare that they have no known competing financial interests or personal relationships that could have appeared to influence the work reported in this paper.

## Funding

This work is partly supported by the China Postdoctoral Science Foundation (2020M681825), the projects from the 13th Five-Year Plan (No. 17SAZ01 and 18QNP063) and National Natural Science Foundation of China (No. 42171398).

## Authors' contributions

JH and WZ designed this work; YW, PL and WY collected the data; JH implemented formal analysis and drafted the manuscript; XW, HS, YX, SL, RSM, YG and WZ substantively revised the manuscript.

## Credit author statement

Conceptualization: Junyu He and Wenyi Zhang. Data curation: Yong Wang, Ping Liu and Wenwu Yin. Formal analysis: Junyu He. Writing-original draft: Junyu He. Writing-review & editing: Xianyu Wei, Hailong Sun, Yuanyong Xu, Shanshan Li, Ricardo J. Soares Magalhaes, Yuming Guo and Wenyi Zhang.

## Data availability

The authors do not have permission to share data.

## Acknowledgements

Not applicable.

## Appendix A

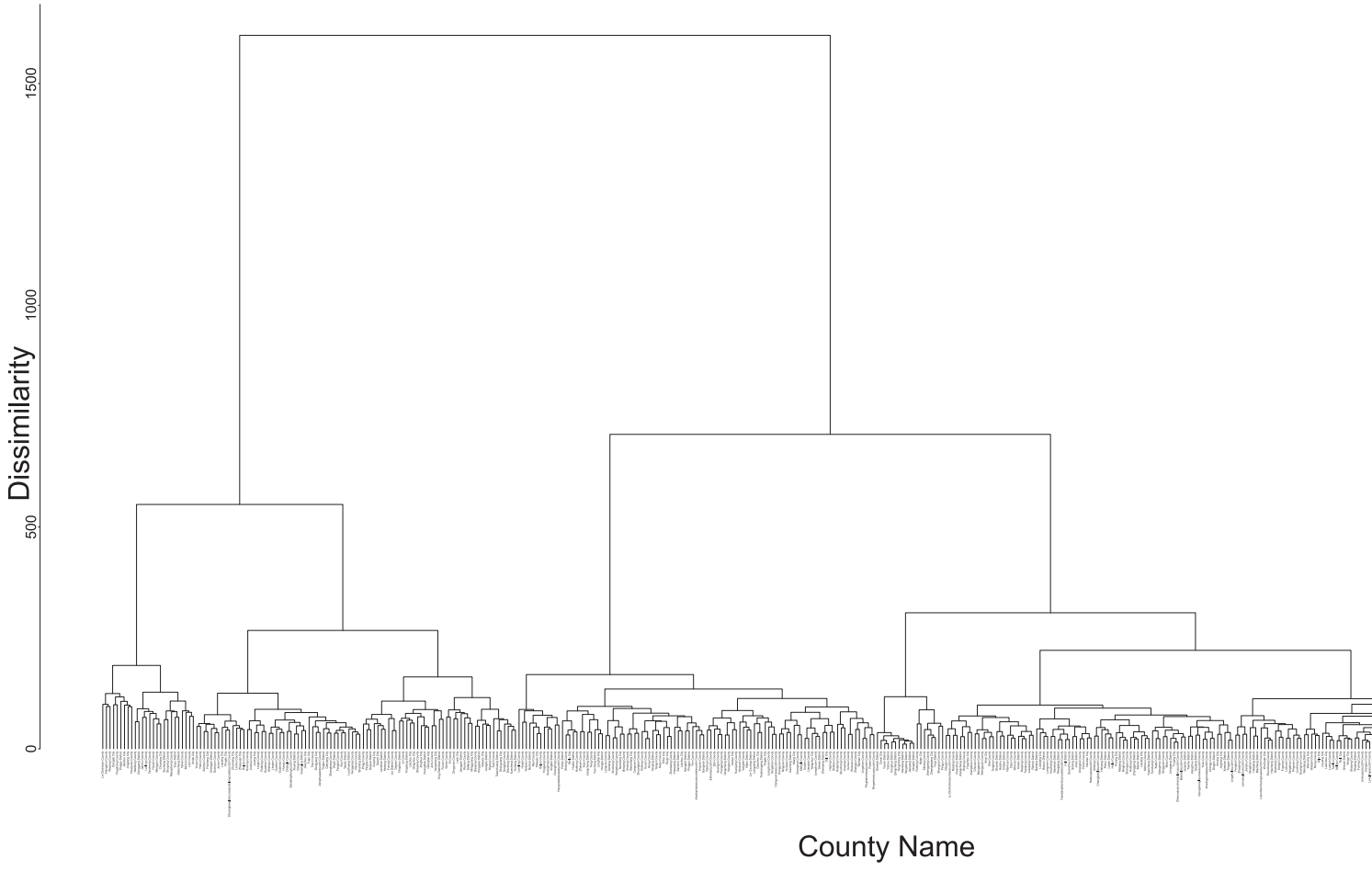


**Fig. A1.** Cluster tree of the wavelet power spectra at 434 counties.

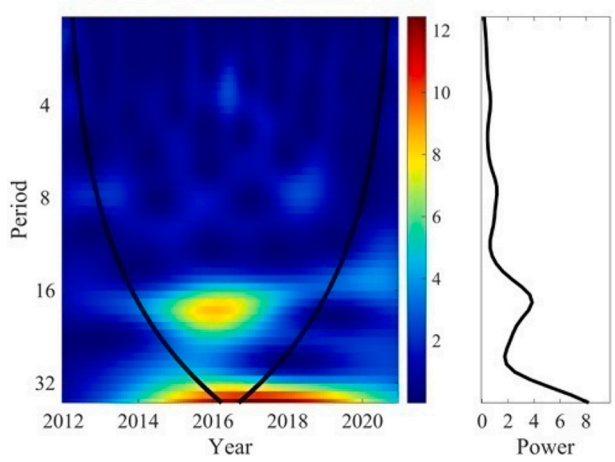


**Fig. A2.** Wavelet power spectra of the multivariate ENSO index. The left part of each subfigure represents the wavelet power spectrum at time-frequency domain, while the right part represents the global averaged power values at corresponding frequency domain. Black lines in the spectra represent the significant areas at the 5% level, and the color from blue to red display the low to high wavelet power values, indicating the cyclic strength. (For interpretation of the references to color in this figure legend, the reader is referred to the web version of this article.)

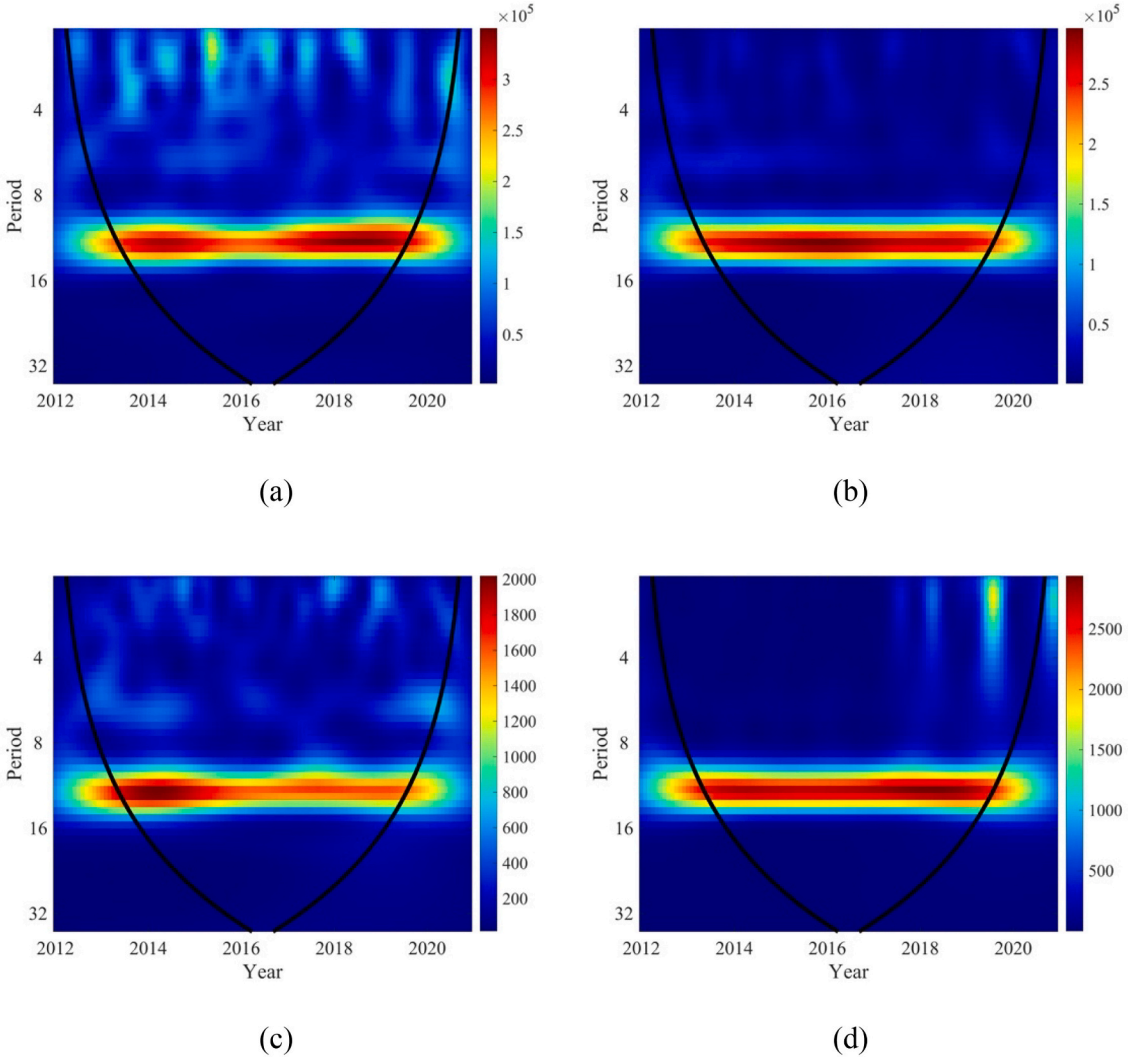


**Fig. A3.** Averaged wavelet power spectra of (a) precipitation, (b) pressure, (c) relative humidity and (d) temperature in the studied counties.

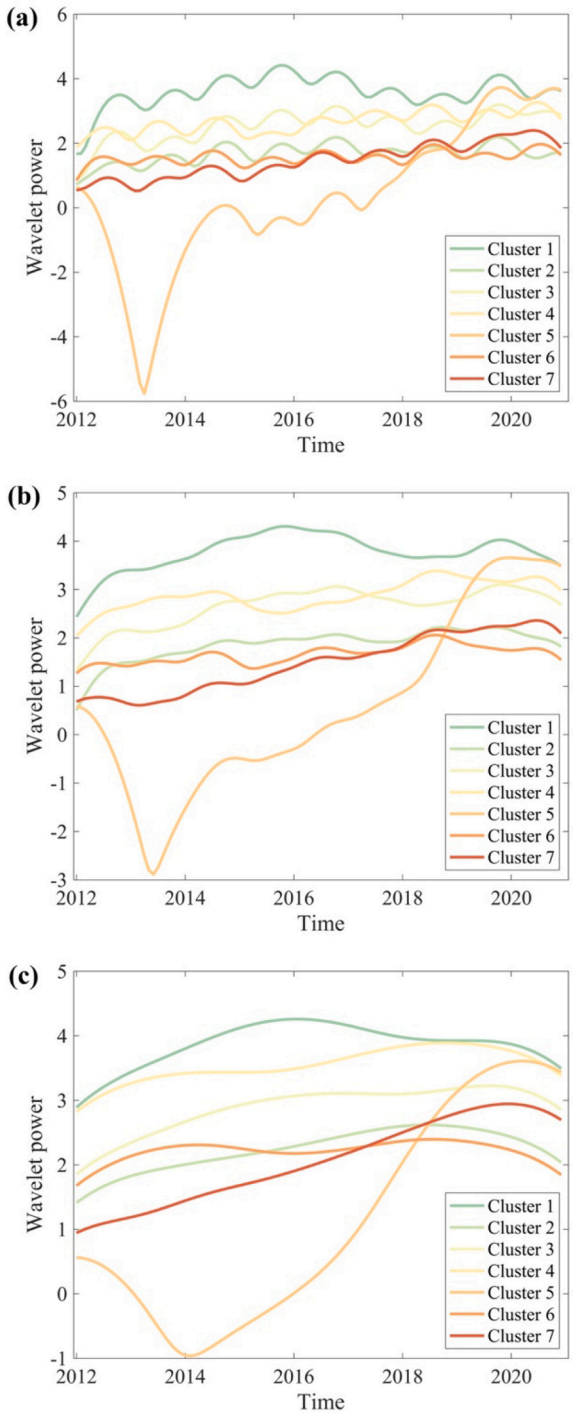


**Fig. A4.** The series of wavelet power values at (a) 4-month period, (b) 6-month period, (c) 12-month period for the seven clusters.

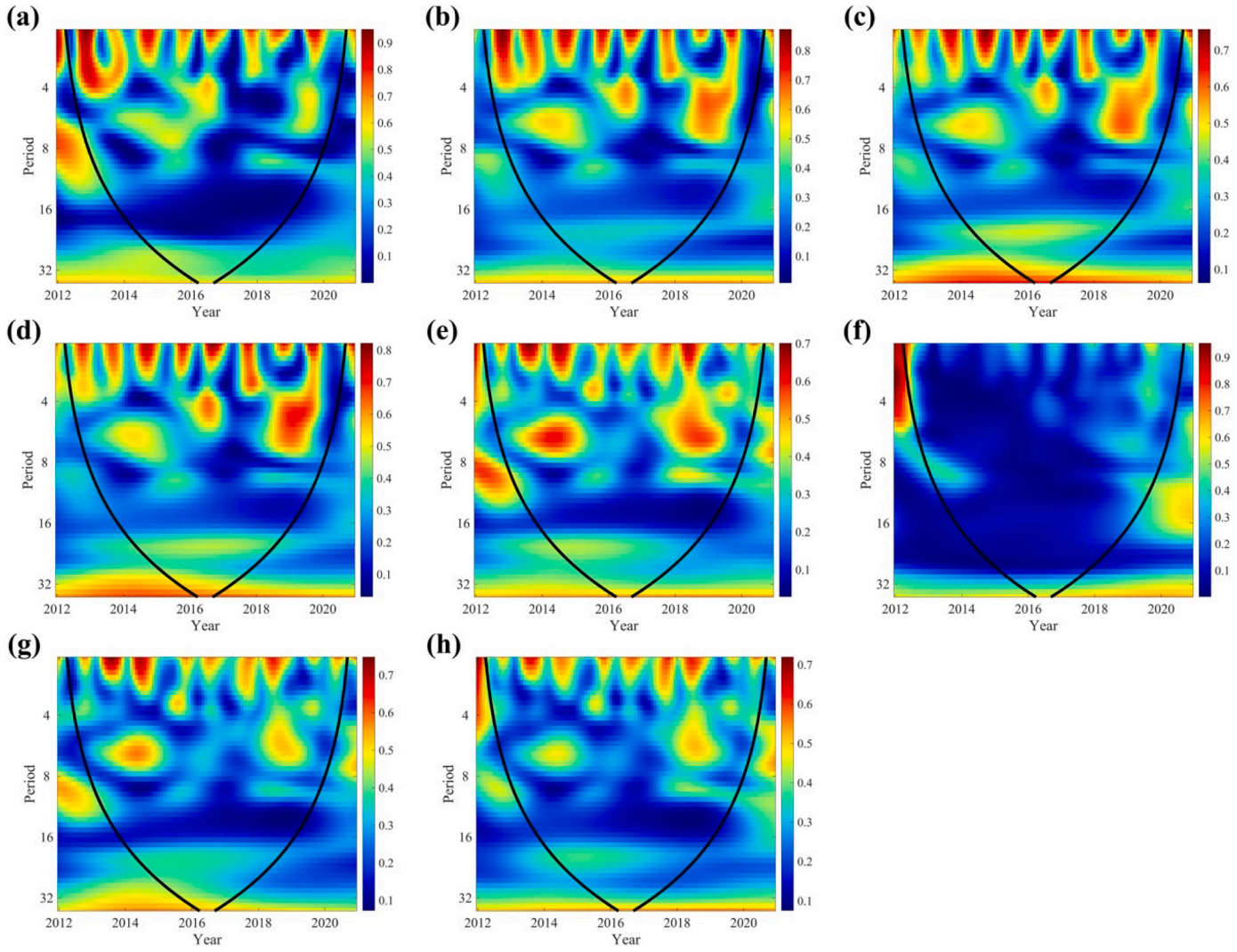


**Fig. A5.** Averaged wavelet coherency spectra between the Scrub typhus cases and Niño 3.4 SST index for (a) the entire mainland China and (b-h) the seven clusters. Black lines in the spectra represent the significant areas at the 5% level, and the color from blue to red display the low to high wavelet coherency values, indicating the strength of co-variation between Scrub typhus cases and Niño 3.4 SST index. (For interpretation of the references to color in this figure legend, the reader is referred to the web version of this article.)

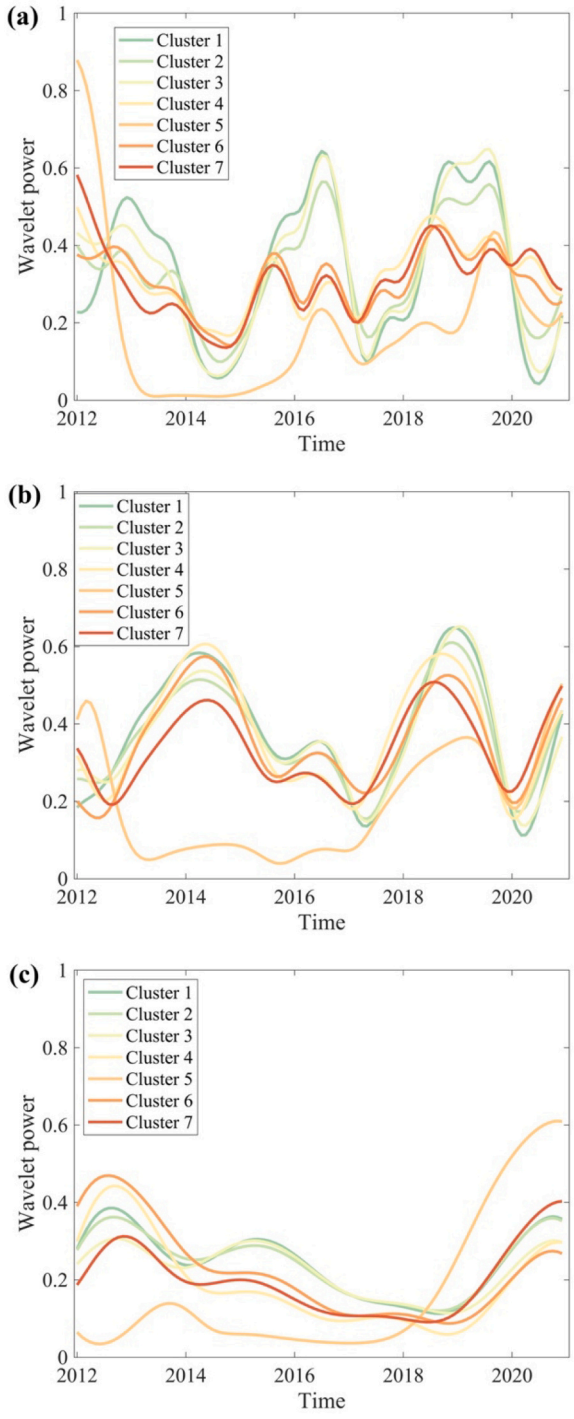


**Fig. A6.** The series of wavelet coherency values between Scrub typhus cases and Niño 3.4 SST index at (a) 4-month period, (b) 6-month period, (c) 12-month period for the seven clusters.

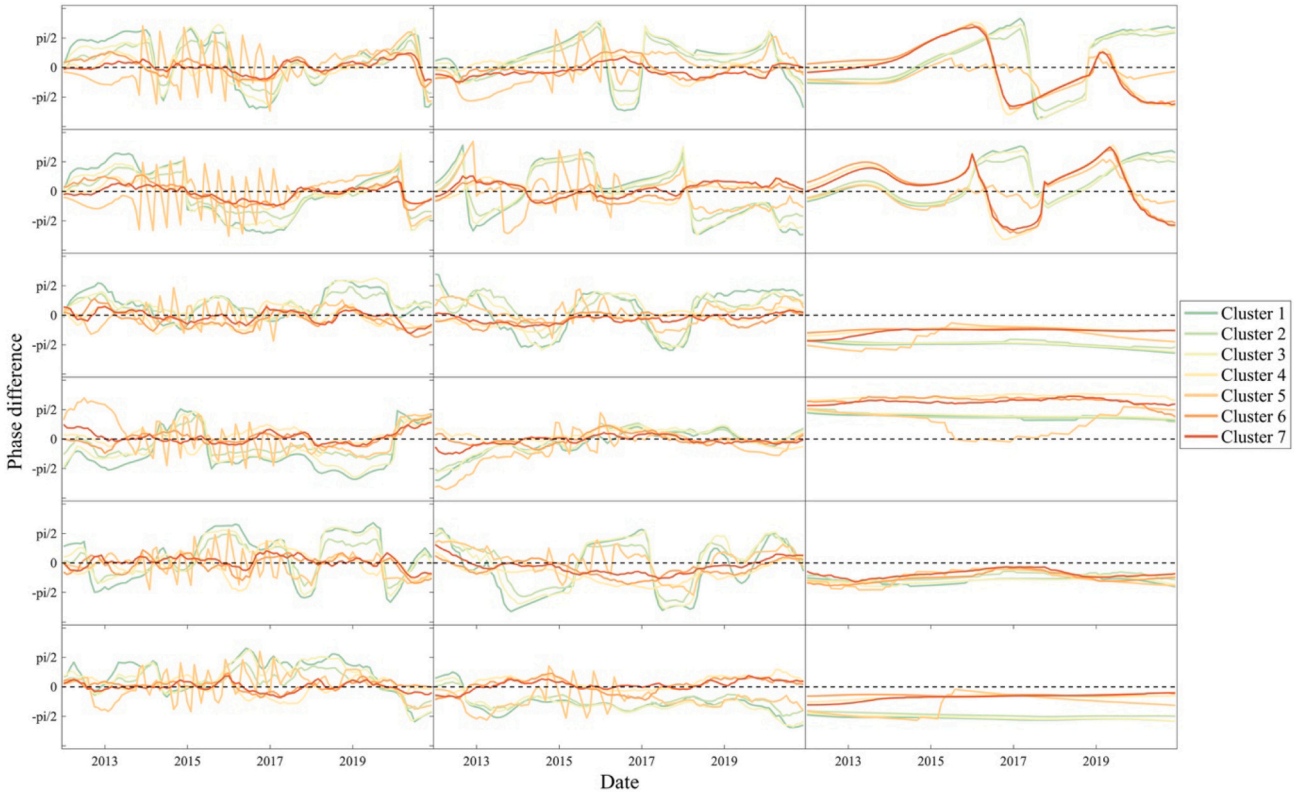


**Fig. A7.** Phase difference between Scrub Typhus cases and six environmental variables (including Niño 3.4 SST index, multivariate El Niño Southern Oscillation index, precipitation, pressure, relative humidity, temperature in Row 1 to 6, respectively) at three temporal periods (including 4, 6, 12-month period in Column 1 to 3, respectively).

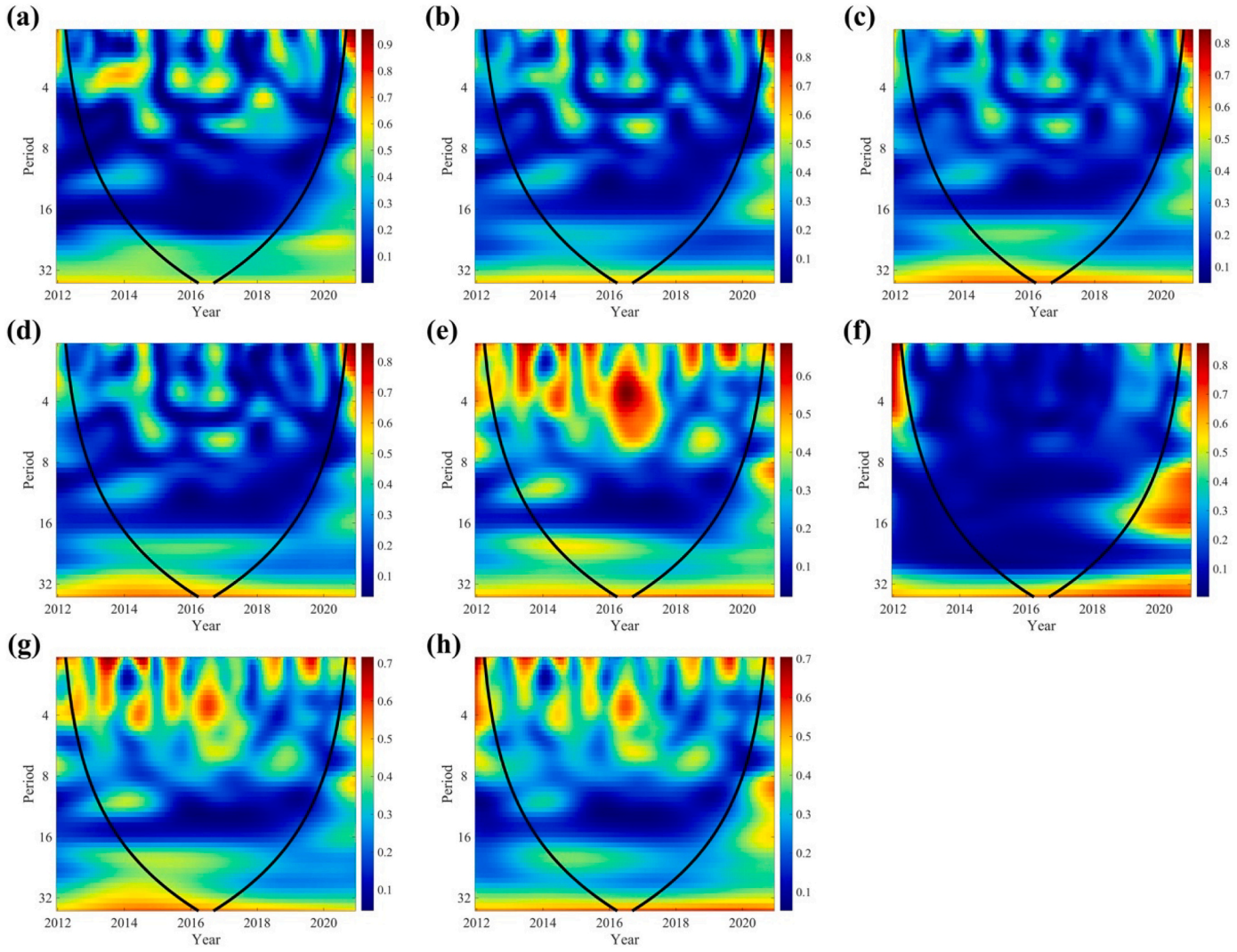


**Fig. A8.** Averaged wavelet coherency spectra between the Scrub typhus cases and multivariate ENSO index for (a) the entire mainland China and (b-h) the seven clusters. Black lines in the spectra represent the significant areas at the 5% level, and the color from blue to red display the low to high wavelet coherency values, indicating the strength of co-variation between Scrub typhus cases and multivariate ENSO index. (For interpretation of the references to color in this figure legend, the reader is referred to the web version of this article.)

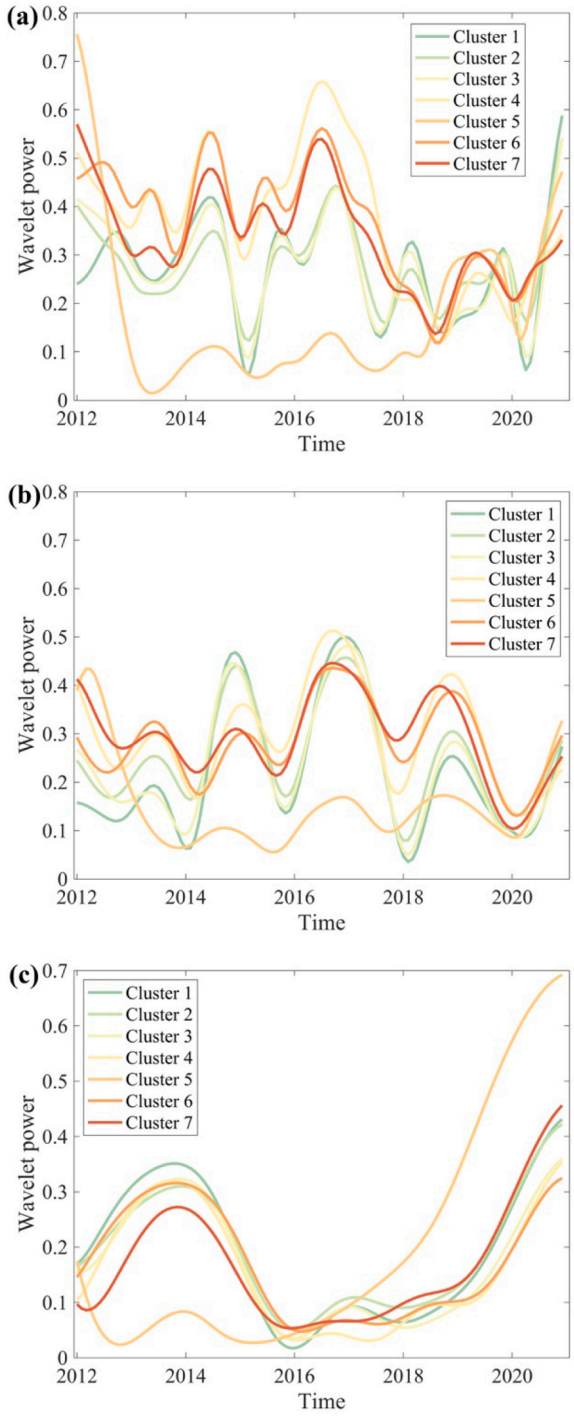


**Fig. A9.** The series of wavelet coherency values between the Scrub typhus cases and multivariate ENSO index at (a) 4-month period, (b) 6-month period, (c) 12-month period for the seven clusters.

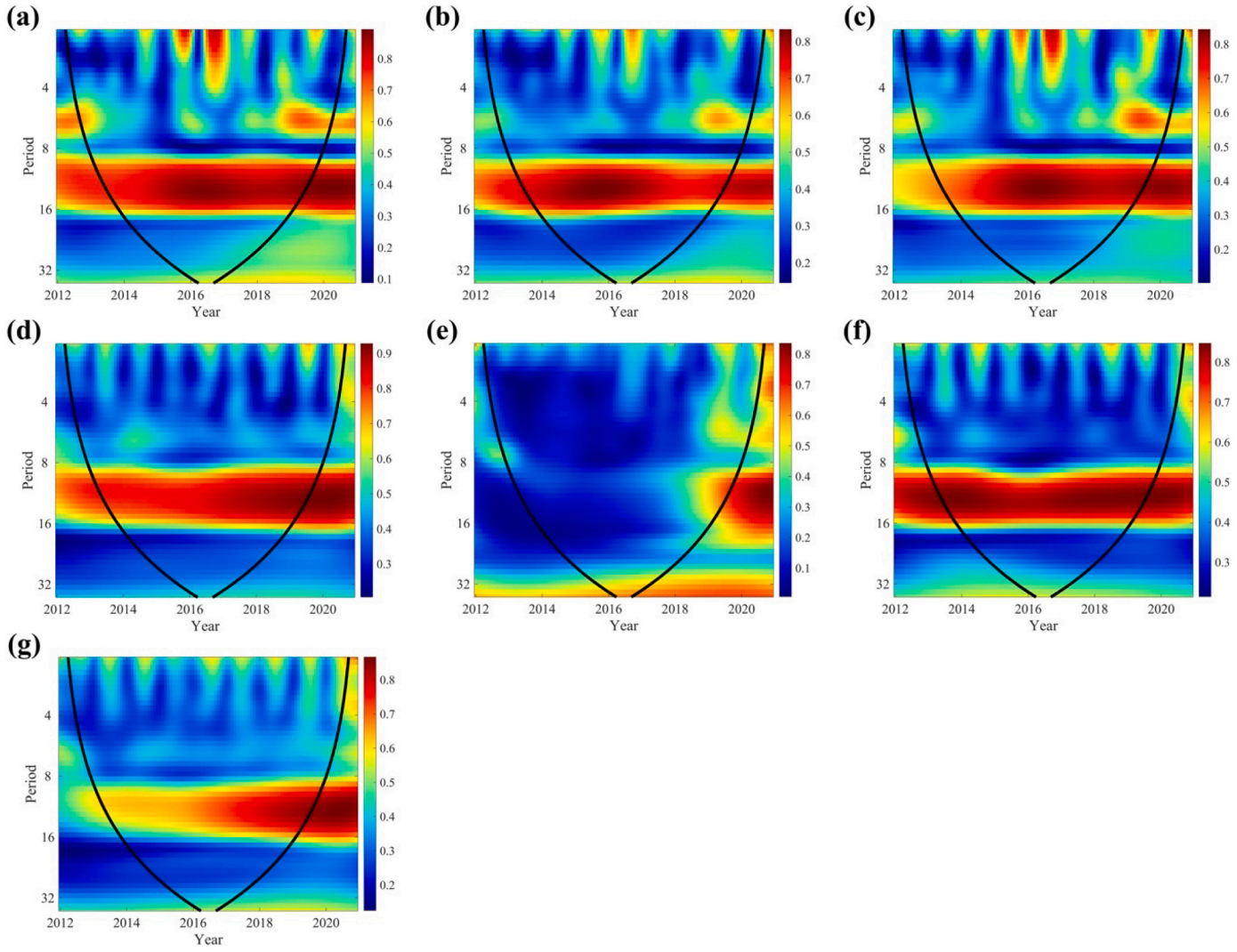


**Fig. A10.** Averaged wavelet coherency spectra between the Scrub typhus cases and precipitation for (a-g) the seven clusters. Black lines in the spectra represent the significant areas at the 5% level, and the color from blue to red display the low to high wavelet coherency values, indicating the strength of co-variation between Scrub typhus cases and precipitation. (For interpretation of the references to color in this figure legend, the reader is referred to the web version of this article.)

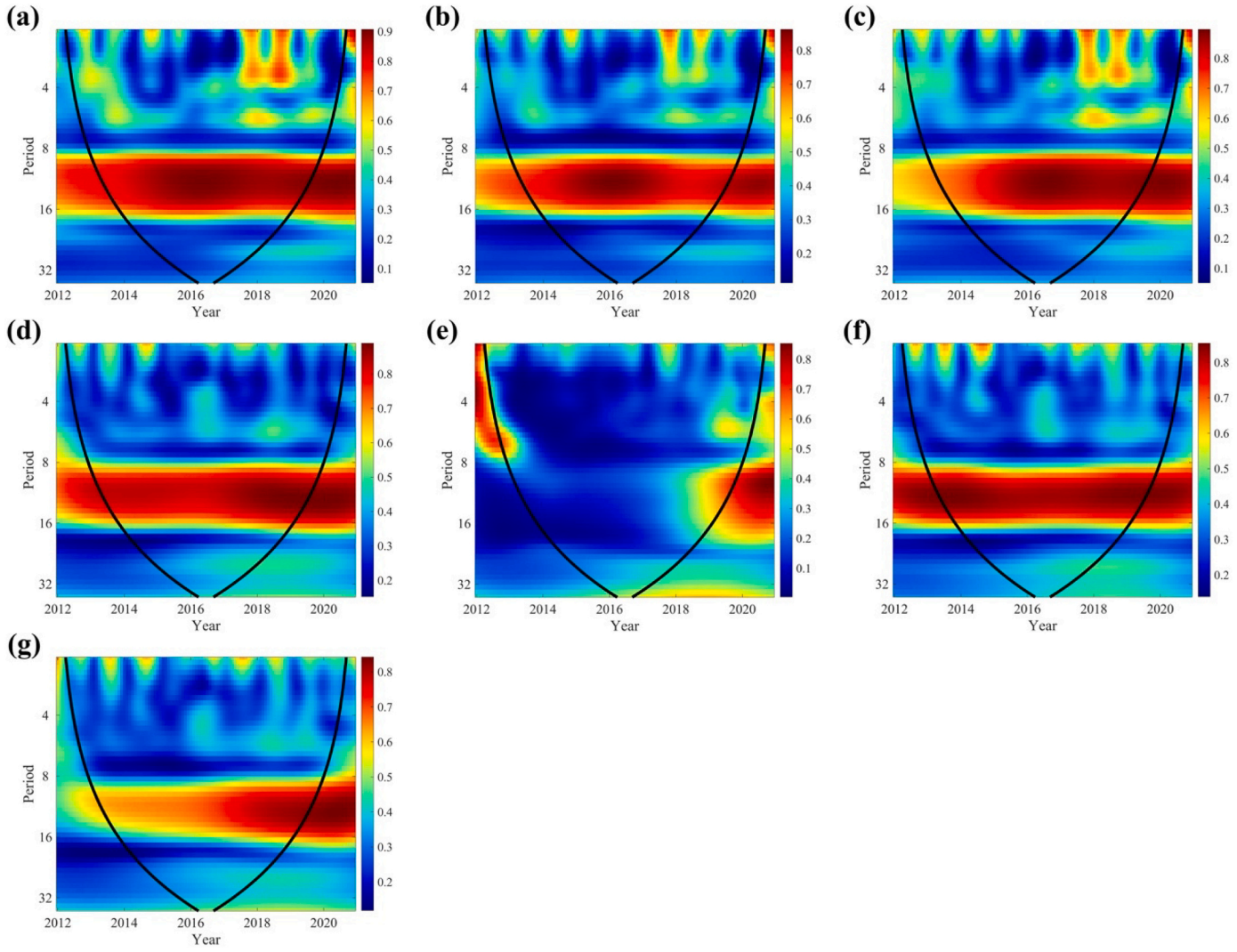


**Fig. A11.** Averaged wavelet coherency spectra between the Scrub typhus cases and pressure for (a-g) the seven clusters. Black lines in the spectra represent the significant areas at the 5% level, and the color from blue to red display the low to high wavelet coherency values, indicating the strength of co-variation between Scrub typhus cases and pressure. (For interpretation of the references to color in this figure legend, the reader is referred to the web version of this article.)

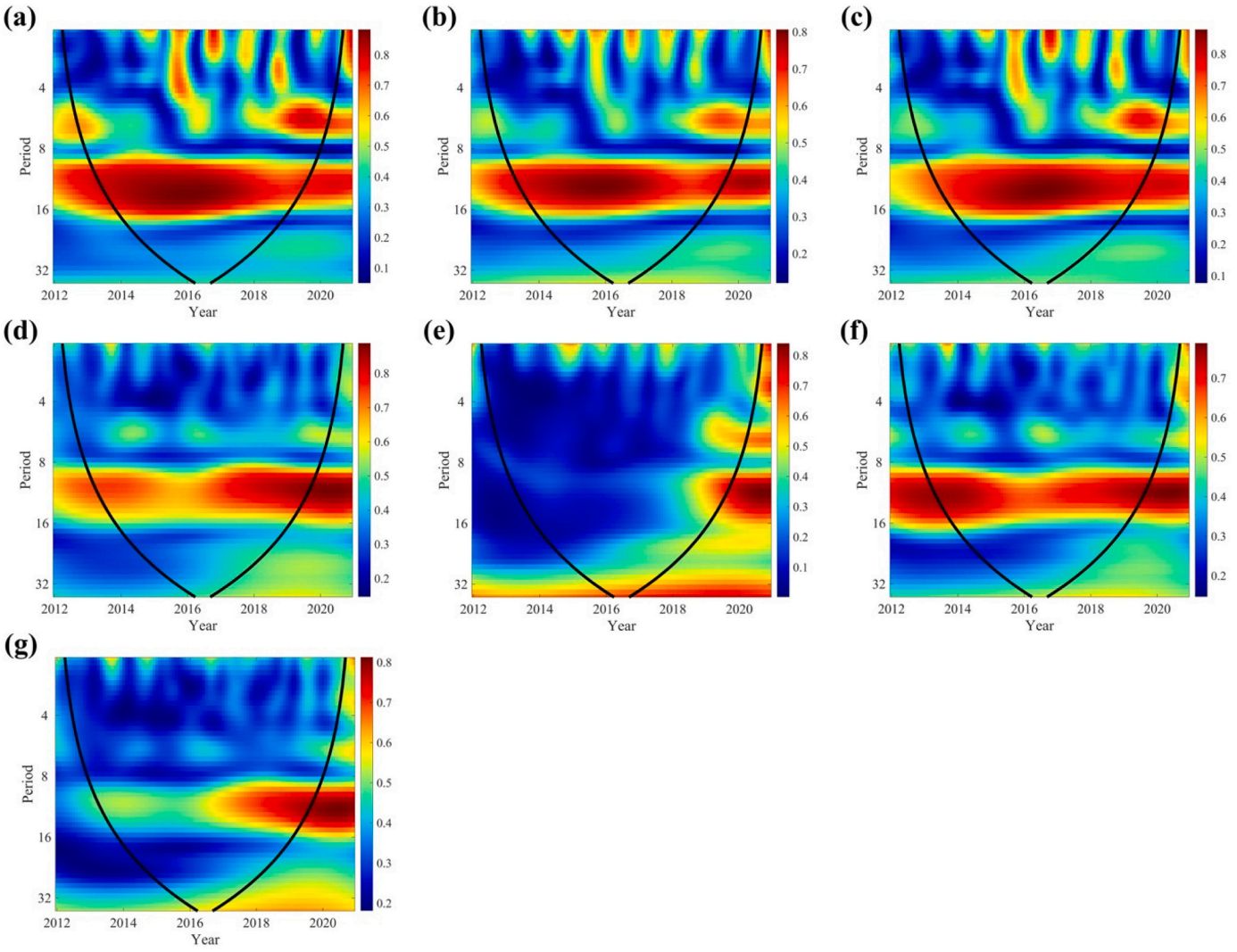


**Fig. A12.** Averaged wavelet coherency spectra between the Scrub typhus cases and relative humidity for (a-g) the seven clusters. Black lines in the spectra represent the significant areas at the 5% level, and the color from blue to red display the low to high wavelet coherency values, indicating the strength of co-variation between Scrub typhus cases and relative humidity. (For interpretation of the references to color in this figure legend, the reader is referred to the web version of this article.)

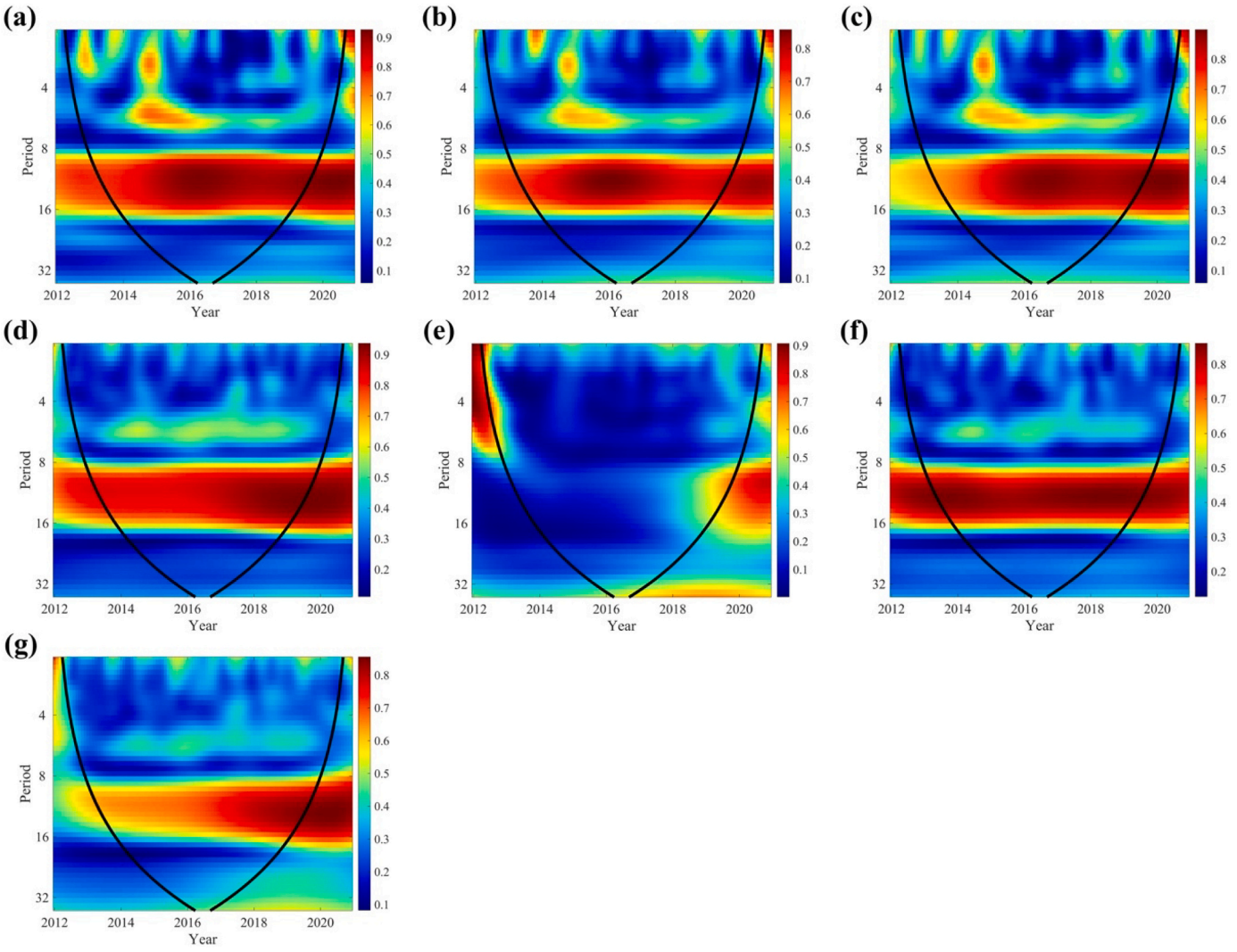


**Fig. A13.** Averaged wavelet coherency spectra between the Scrub typhus cases and temperature for (a-g) the seven clusters. Black lines in the spectra represent the significant areas at the 5% level, and the color from blue to red display the low to high wavelet coherency values, indicating the strength of co-variation between Scrub typhus cases and temperature. (For interpretation of the references to color in this figure legend, the reader is referred to the web version of this article.)

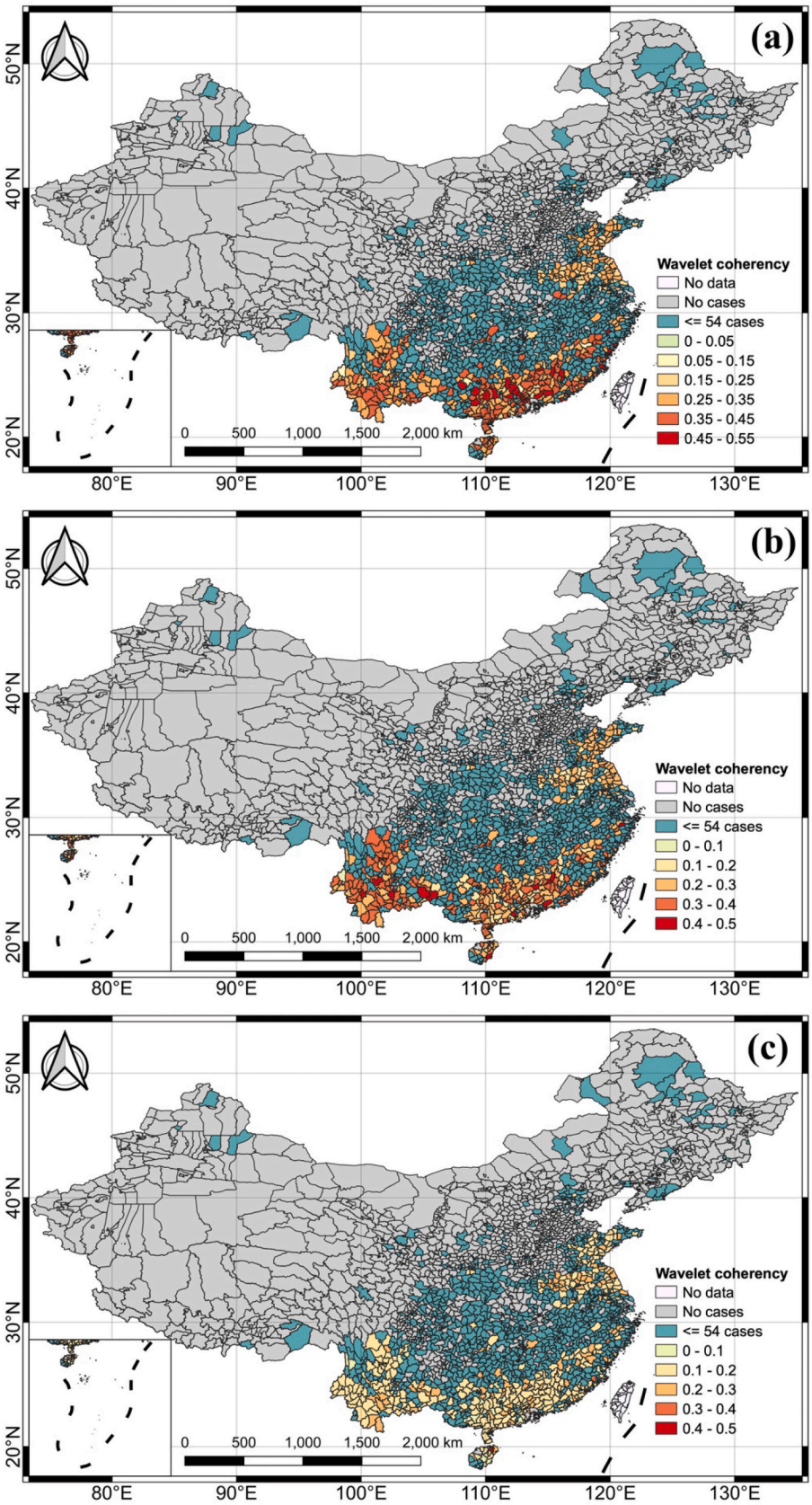


**Fig. A14.** Maps of the averaged association strength between the Scrub typhus cases and multivariate ENSO index during the period 2012–2020 at (a) 4-month period, (b) 6-month period, (c) 12-month period.

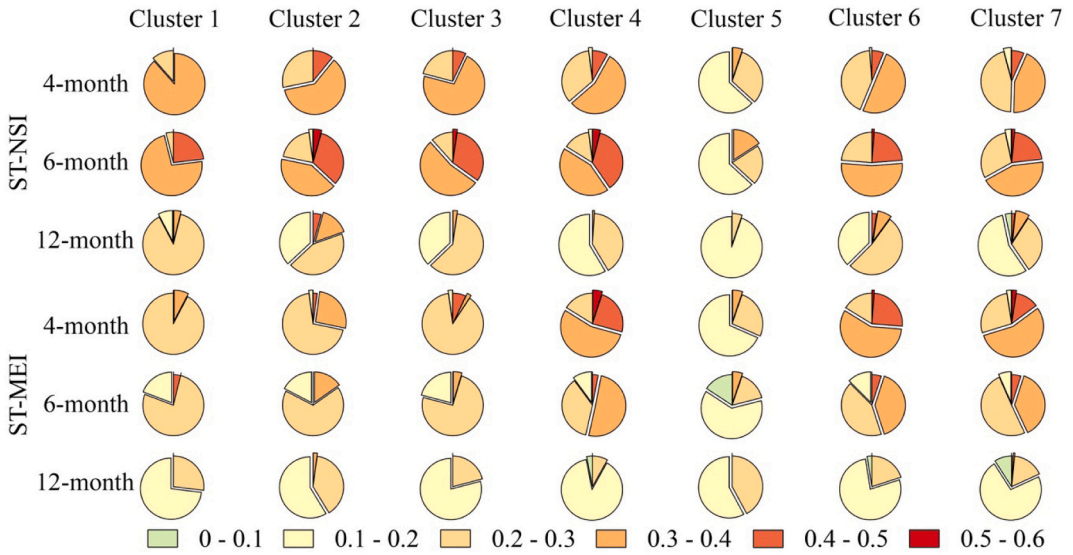


**Fig. A15.** Proportions of counties for each cluster with various mean coherency values between the Scrub typhus cases and Niño 3.4 SST index, or between the Scrub typhus cases and multivariate ENSO index.

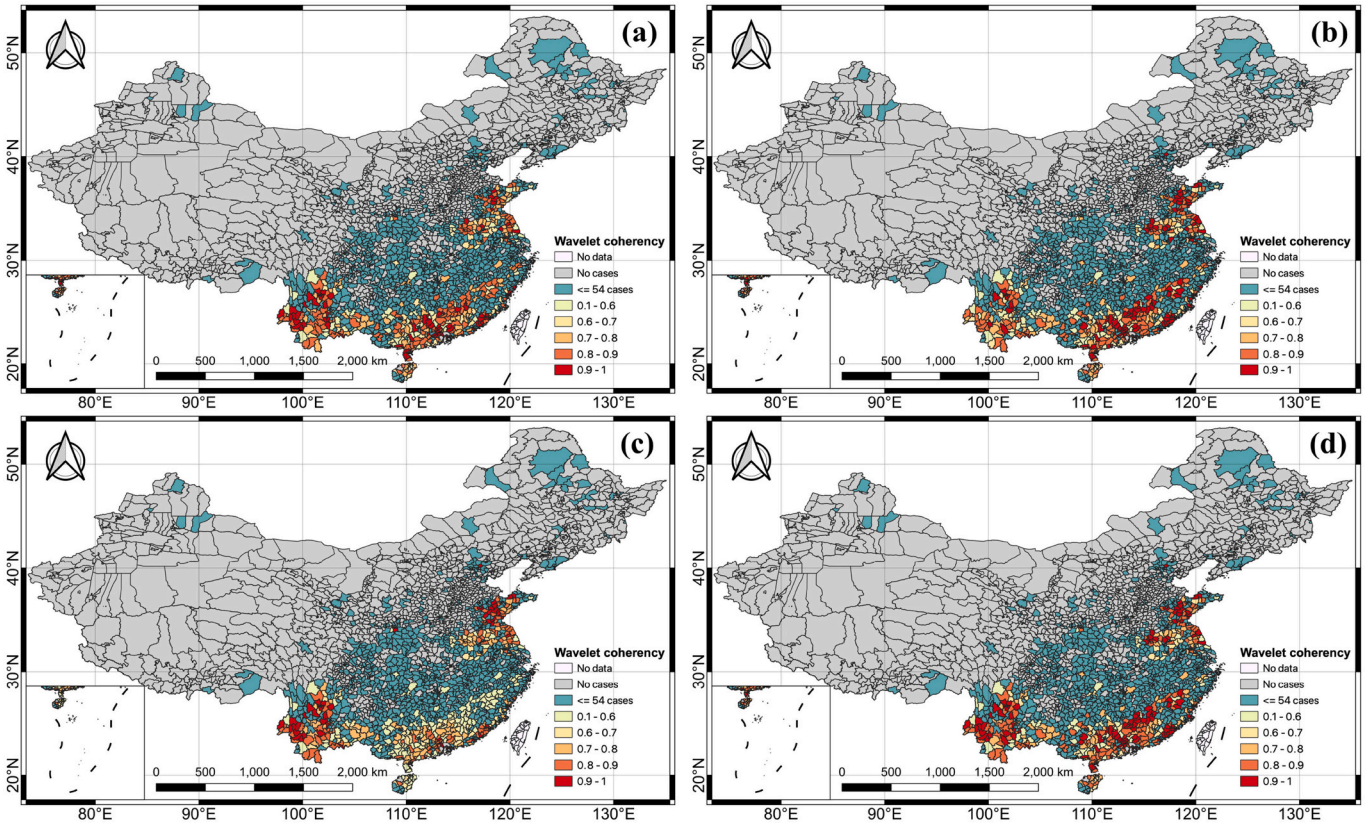


**Fig. A16.** Maps of the averaged association strength between the Scrub typhus cases and (a) precipitation, (b) pressure, (c) relative humidity, (d) temperature during the period 2012–2020 at 12-month period.

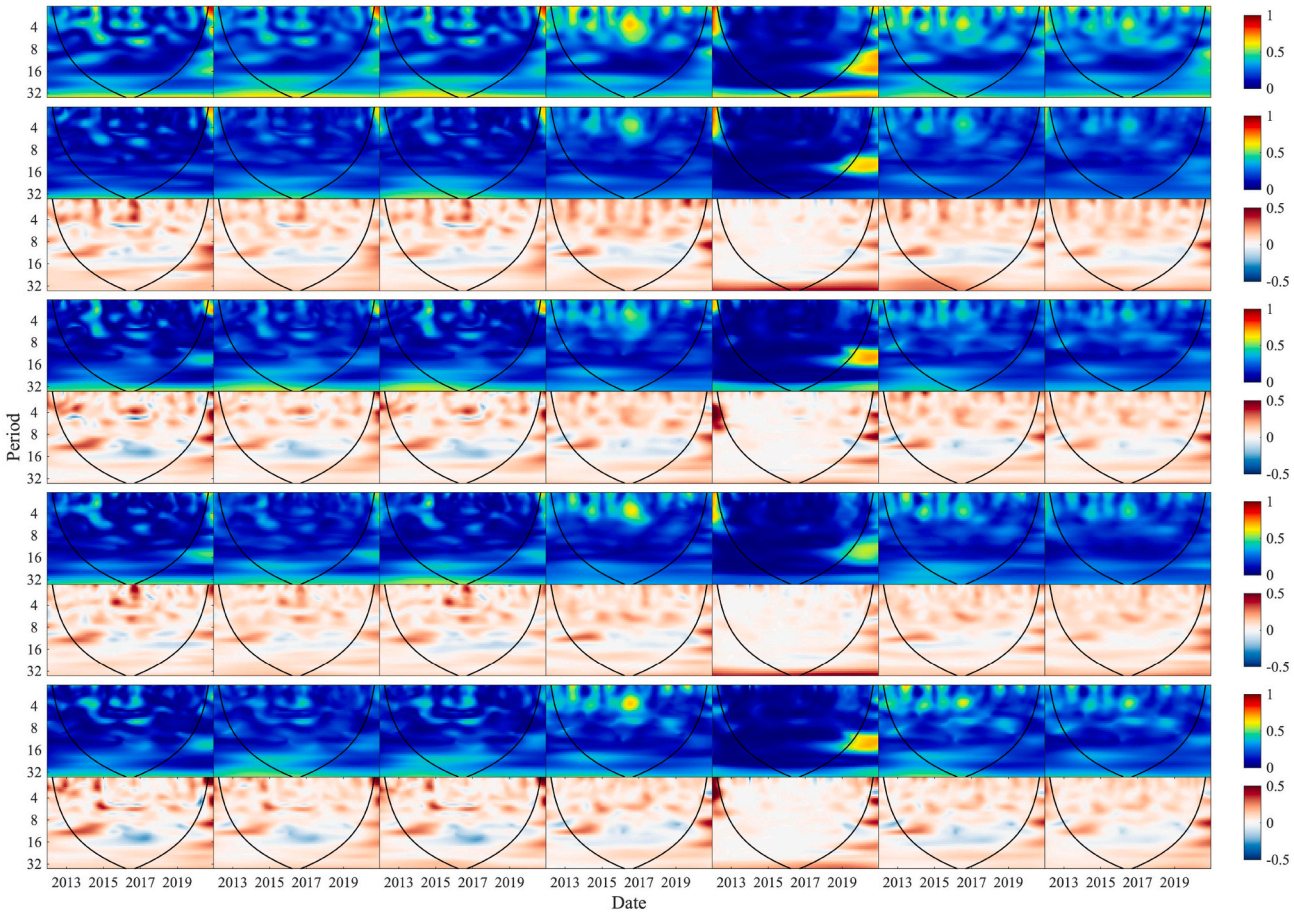


**Fig. A17.** Wavelet coherency spectra and partial wavelet coherency spectra. The subplots in Row 1 represent the wavelet coherency spectra between multivariate El Niño Southern Oscillation index and Scrub Typhus cases for each of the seven clusters; the subplots in Row 2, 4, 6, 8 represent the partial wavelet coherency spectra between multivariate El Niño Southern Oscillation index and Scrub Typhus cases excluding the effects of precipitation, pressure, relative humidity and temperature, respectively, for each of the seven clusters; the subplots in Row 3, 5, 7, 9, represents the spectra difference between the spectra in Row 1 and Row 2, 4, 6, 8, respectively.

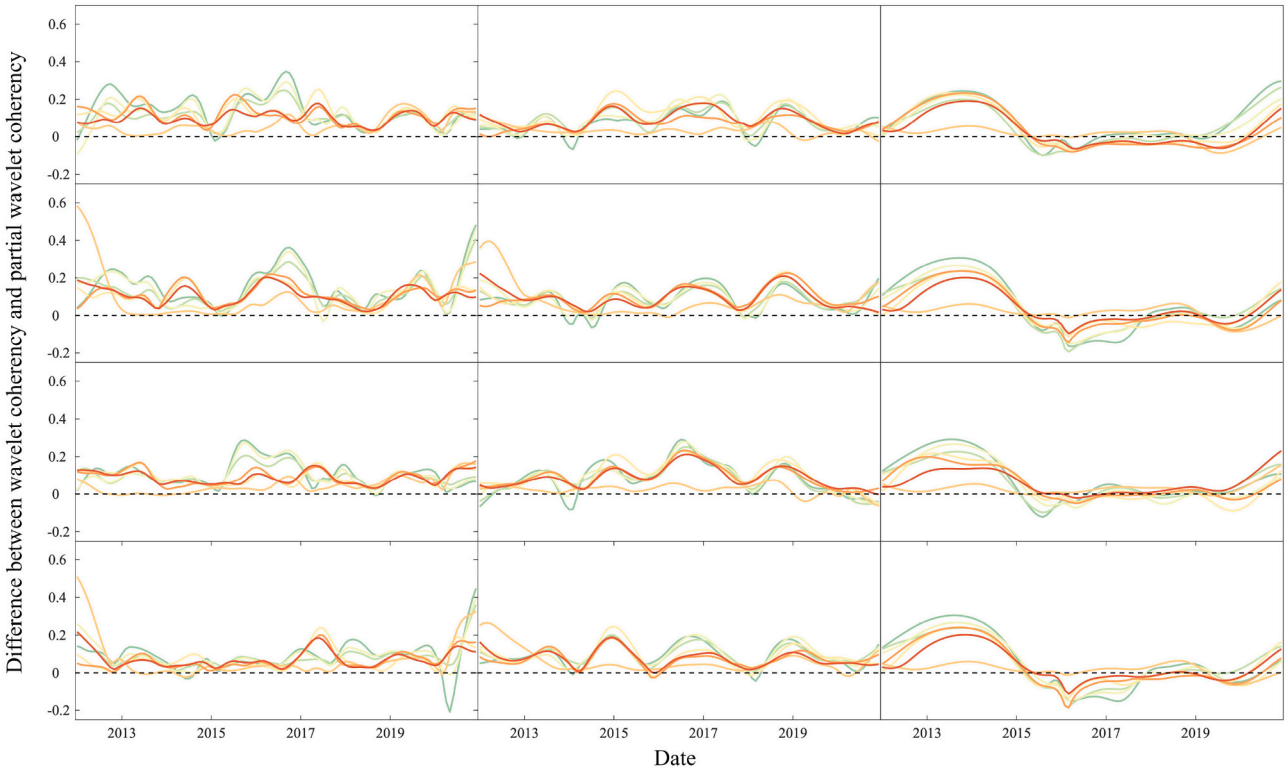


**Fig. A18.** Spectra difference between wavelet coherency spectra for multivariate El Niño Southern Oscillation index-Scrub Typhus cases association and partial wavelet coherency spectra for the association excluding the effects of four meteorological variables. The subplots from Row 1 to 4 respectively represent the spectra difference for precipitation, pressure, relative humidity, temperature; while the subplots from Column 1 to 3 represent the spectra difference at 4, 6, and 12-month period, respectively.

## References


[1] R. Premaratna, T.G.A.N. Chandrasena, A.S. Dassayake, A.D. Loftis, G.A. Dasch, H. J. de Silva, Acute hearing loss due to scrub typhus: a forgotten complication of a reemerging disease, Clin. Infect. Dis. 42 (2006) e6–e8, https://doi.org/10.1086/498747.

[2] H.C. Kim, I.Y. Lee, S.T. Chong, A.L. Richards, S.H. Gu, J.W. Song, J.S. Lee, T. A. Klein, Serosurveillance of scrub typhus in small mammals collected from military training sites near the DMZ, Northern Gyeonggi-do, Korea, and analysis of the relative abundance of chiggers from mammals examined, Korean J. Parasitol. 48 (2010) 237–243, https://doi.org/10.3347/kjp.2010.48.3.237.

[3] L.W.J. Sames, C.T.A. Klein, H.-C. Kim, S.H. Gu, H.-J. Kang, S.-H. Shim, S.-J. Ha, S.-T. Chong, I.-Y. Lee, A.L. Richards, S.-H. Yi, J.-W. Song, Serological surveillance of scrub typhus, murine typhus, and leptospirosis in small mammals captured at twin bridges training area, Gyeonggi Province, Republic of Korea, 2005–2007, Mil. Med. 175 (2010) 7.

[4] B. Bhopdhornangkul, A.C. Meeyai, W. Wongwit, Y. Limpanont, S. Iamsirithaworn, Y. Laosiritaworn, K. Tantrakarnapa, Non-linear effect of different humidity types on scrub typhus occurrence in endemic provinces, Thailand, Heliyon 7 (2021), e06095, https://doi.org/10.1016/j.heliyon.2021.e06095.

[5] Y. Wu, Q. Qian, R.J. Magalhaes, Z.H. Han, U. Haque, T.A. Weppelmann, W.B. Hu, Y.X. Liu, Y.S. Sun, W.Y. Zhang, S.L. Li, Rapid increase in scrub typhus incidence in mainland China, 2006-2014, Am. J. Trop. Med. Hyg. 94 (2016) 532–536, https://doi.org/10.4269/ajtmh.15-0663.

[6] Z. Li, H. Xin, J. Sun, S. Lai, L. Zeng, C. Zheng, S.E. Ray, N.D. Weaver, L. Wang, J. Yu, Z. Feng, S.I. Hay, G.F. Gao, Epidemiologic changes of scrub typhus in China, 1952-2016, Emerg. Infect. Dis. 26 (2020) 1091–1101, https://doi.org/10.3201/eid2606.191168.

[7] S. Zhang, H. Song, Y. Liu, Q. Li, Y. Wang, J. Wu, J. Wan, G. Li, C. Yu, X. Li, W. Yin, Z. Xu, B. Liu, Q. Zhang, K. Wan, G. Li, X. Fu, J. Zhang, J. He, R. Hai, D. Yu, D. H. Walker, J. Xu, X.J. Yu, Scrub typhus in previously unrecognized areas of endemicity in China, J. Clin. Microbiol. 48 (2010) 1241–1244, https://doi.org/10.1128/JCM.01784-09.

[8] H. Yao, Y. Wang, X. Mi, Y. Sun, K. Liu, X. Li, X. Ren, M. Geng, Y. Yang, L. Wang, W. Liu, L. Fang, The scrub typhus in mainland China: spatiotemporal expansion and risk prediction underpinned by complex factors, Emerg. Microb. Infect. 8 (2019) 909–919, https://doi.org/10.1080/22221751.2019.1631719.

[9] Y. Wu, Q. Qian, R.J.S. Magalhaes, Z.-H. Han, W.-B. Hu, U. Haque, T. A. Weppelmann, Y. Wang, Y.-X. Liu, X.-L. Li, H.-L. Sun, Y.-S. Sun, A.C.A. Clements, S.-L. Li, W.-Y. Zhang, Spatiotemporal dynamics of scrub typhus transmission in Mainland China, 2006-2014, PLoSNegl. Trop. Dis. 10 (2016), e0004875, https://doi.org/10.1371/journal.pntd.0004875.

[10] Y. Yue, D. Ren, X. Liu, Y. Wang, Q. Liu, G. Li, Spatio-temporal patterns of scrub typhus in mainland China, 2006-2017, PLoSNegl. Trop. Dis. 13 (2019), e0007916, https://doi.org/10.1371/journal.pntd.0007916.

[11] B. Cazelles, M. Chavez, G.C. de Magny, J.-F. Guégan, S. Hales, Time-dependent spectral analysis of epidemiological time-series with wavelets, J. R. Soc. Interface 4 (2007) 625–636.

[12] A.M. Holdsworth, N.K.-R. Kevlahan, D.J.D. Earn, Multifractal signatures of infectious diseases, J. R. Soc. Interface 9 (2012) 2167–2180.

[13] K.T.D. Thai, B. Cazelles, N.V. Nguyen, L.T. Vo, M.F. Boni, J. Farrar, C.P. Simmons, H.R. van Doorn, P.J. de Vries, Dengue dynamics in BinhThuan Province, Southern Vietnam: periodicity, synchronicity and climate variability, PLoSNegl. Trop. Dis. 4 (2010), e747, https://doi.org/10.1371/journal.pntd.0000747.

[14] H.Q. Cuong, N.T. Vu, B. Cazelles, M.F. Boni, K.T.D. Thai, M.A. Rabaa, L.C. Quang, C.P. Simmons, T.N. Huu, K.L. Anders, Spatiotemporal dynamics of dengue epidemics, southern Vietnam, Emerg. Infect. Dis. 19 (2013) 945–953, https://doi.org/10.3201/eid1906.121323.

[15] Tristan Rouyer, J.-M. Fromentin, N.C. Stenseth, B. Cazelles, Analysing multiple time series and extending significance testing in wavelet analysis, Mar. Ecol. Prog. Ser. 359 (2008) 11–23, https://doi.org/10.3354/meps07330.

[16] T. Rouyer, J.-M. Fromentin, F. Ménard, B. Cazelles, K. Briand, R. Pianet, B. Planque, N.C. Stenseth, Complex interplays among population dynamics, environmental forcing, and exploitation in fisheries, Proc. Natl. Acad. Sci. 105 (2008) 5420–5425.

[17] E. Benincà, M. van Boven, T. Hagenaars, W. van der Hoek, Space-time analysis of pneumonia hospitalisations in the Netherlands, PLoS One 12 (2017), e0180797.

[18] J. Seto, Y. Suzuki, R. Nakao, K. Otani, K. Yahagi, K. Mizuta, Meteorological factors affecting scrub typhus occurrence: a retrospective study of Yamagata prefecture, Japan, 1984-2014, Epidemiol. Infect. 145 (2017) 462–470, https://doi.org/10.1017/S0950268816002430.

[19] Y. Wei, Y. Huang, X. Li, Y. Ma, X. Tao, X. Wu, Z. Yang, Climate variability, animal reservoir and transmission of scrub typhus in Southern China, PLoSNegl. Trop. Dis. 11 (2017), e0005447, https://doi.org/10.1371/journal.pntd.0005447.

[20] B. Cazelles, M. Chavez, A.J. McMichael, S. Hales, Nonstationary influence of El Niño on the synchronous dengue epidemics in Thailand, PLoS Med. 2 (2005), e106.

[21] J. He, G. Christakos, W. Zhang, Y. Wang, A space-time study of hemorrhagic fever with renal syndrome (HFRS) and its climatic associations in Heilongjiang province, China, Front. Appl. Math. Stat. 3 (2017) 16, https://doi.org/10.3389/fams.2017.00016.

[22] J. He, G. Christakos, J. Wu, B. Cazelles, Q. Qian, D. Mu, Y. Wang, W. Yin, W. Zhang, Spatiotemporal variation of the association between climate dynamics and HFRS outbreaks in Eastern China during 2005-2016 and its geographic determinants, PLoSNegl. Trop. Dis. 12 (2018), e0006554, https://doi.org/10.1371/journal.pntd.0006554.
[23] S.H. Kang, R.P. McIver, J.A. Hernandez, Co-movements between bitcoin and gold: a wavelet coherence analysis, Phys. Stat. Mech. Its Appl. 536 (2019), 120888.
[24] X. Xiao, J. He, Y. Yu, B. Cazelles, M. Li, Q. Jiang, C. Xu, Teleconnection between phytoplankton dynamics in north temperate lakes and global climatic oscillation by time-frequency analysis, Water Res. 154 (2019) 267–276, https://doi.org/10.1016/j.watres.2019.01.056.
[25] B. Blasius, L. Stone, Nonlinearity and the Moran effect, Nature 406 (2000) 846–847, https://doi.org/10.1038/35022646.
[26] P. Moran, The statistical analysis of the Canadian Lynx cycle, Aust. J. Zool. 1 (1953) 291–298, https://doi.org/10.1071/zo9530291.
[27] H. Yu, C. Sun, W. Liu, Z. Li, Z. Tan, X. Wang, J. Hu, S. Shi, C. Bao, Scrub typhus in Jiangsu Province, China: epidemiologic features and spatial risk analysis, BMC Infect. Dis. 18 (2018) 372, https://doi.org/10.1186/s12879-018-3271-x.
[28] E.E. Goldwyn, A. Hastings, The roles of the Moran effect and dispersal in synchronizing oscillating populations, J. Theor. Biol. 289 (2011) 237–246.
[29] W.D. Koenig, Spatial autocorrelation of ecological phenomena, Trends Ecol. Evol. 14 (1999) 22–26.
[30] B.K. Acharya, W. Chen, Z. Ruan, G.P. Pant, Y. Yang, L.P. Shah, C. Cao, Z. Xu, M. Dhimal, H. Lin, Mapping environmental suitability of scrub typhus in Nepal using MaxEnt and random forest models, Int. J. Environ. Res. Public Health 16 (2019) 4845.
[31] C. Zheng, D. Jiang, F. Ding, J. Fu, M. Hao, Spatiotemporal patterns and risk factors for scrub typhus from 2007 to 2017 in southern China, Clin. Infect. Dis. 69 (2019) 1205–1211, https://doi.org/10.1093/cid/ciy1050.
[32] J. Kwak, S. Kim, G. Kim, V.P. Singh, S. Hong, H.S. Kim, Scrub typhus incidence modeling with meteorological factors in South Korea, Int. J. Environ. Res. Public Health 12 (2015) 7254–7273, https://doi.org/10.3390/ijerph120707254.
[33] Y.-X. Liu, D. Feng, J.-J. Suo, Y.-B. Xing, G. Liu, L.-H. Liu, H.-J. Xiao, N. Jia, Y. Gao, H. Yang, S.-Q. Zuo, P.-H. Zhang, Z.-T. Zhao, J.-S. Min, P.-T. Feng, S.-B. Ma, S. Liang, W.-C. Cao, Clinical characteristics of the autumn-winter type scrub typhus cases in south of Shandong province, northern China, BMC Infect. Dis. 9 (2009) 82.
[34] C.Y. Wei, J.K. Wang, H.C. Shih, H.C. Wang, C.C. Kuo, Invasive plants facilitated by socioeconomic change harbor vectors of scrub typhus and spotted fever, PLoSNegl. Trop. Dis. 14 (2020), e0007519, https://doi.org/10.1371/journal.pntd.0007519.
[35] J.C. Li, X.Y. Zheng, Z.Y. Xi, Review on the studies of chigger mites and scrub typhus in China, Chin. J. Public Health 16 (2000) 773–775.
[36] G.H. Wu, The epidemiological characteristics and prevention and cure of scrub typhus in China, Chin. J. Public Health 16 (2000) 777–779.
[37] A. Bonell, Y. Lubell, P.N. Newton, J.A. Crump, D.H. Paris, Estimating the burden of scrub typhus: a systematic review, PLoSNegl. Trop. Dis. 11 (2017), e0005838.
[38] S.-S. Kweon, J.-S. Choi, H.-S. Lim, J.-R. Kim, K.-Y. Kim, S.-Y. Ryu, H.-S. Yoo, O. Park, Rapid increase of scrub typhus, South Korea, 2001–2006, Emerg. Infect. Dis. 15 (2009) 1127–1129.
[39] S. Palanivel, K. Nedunchelian, V. Poovazhagi, R. Raghunadan, P. Ramachandran, Clinical profile of scrub typhus in children, Indian J. Pediatr. 79 (2012) 1459–1462.
[40] S.W. Park, N.Y. Ha, B. Ryu, J.H. Bang, H. Song, Y. Kim, G. Kim, M.D. Oh, N.H. Cho, J.K. Lee, Urbanization of scrub typhus disease in South Korea, PLoSNegl. Trop. Dis. 9 (2015), e0003814, https://doi.org/10.1371/journal.pntd.0003814.
[41] Y. Wei, Y. Huang, L. Luo, X. Xiao, L. Liu, Z. Yang, Rapid increase of scrub typhus: an epidemiology and spatial-temporal cluster analysis in Guangzhou City, Southern China, 2006-2012, PLoS One 9 (2014), e101976, https://doi.org/10.1371/journal.pone.0101976.
[42] H. Xin, P. Fu, Junling Sun, S. Lai, W. Hu, A.C.A. Clements, Jianping Sun, J. Cui, S. I. Hay, X. Li, Z. Li, Risk mapping of scrub typhus infections in Qingdao city, China, PLoSNegl. Trop. Dis. 14 (2020), e0008757, https://doi.org/10.1371/journal.pntd.0008757.
[43] M.C. Forchhammer, E. Post, Using large-scale climate indices in climate change ecology studies, Popul. Ecol. 46 (2004) 1–12.
[44] L. Luo, Z. Guo, Z. Lei, Q. Hu, M. Chen, F. Chen, Z. Zhao, J. Rui, X. Liu, Y. Zhu, Y. Wang, M. Yang, T. Chen, Epidemiology of tsutsugamushi disease and its relationship with meteorological factors in Xiamen city, China, PLoSNegl. Trop. Dis. 14 (2020), e0008772.
[45] G.-R. Walther, E. Post, P. Convey, A. Menzel, C. Parmesan, T.J.C. Beebee, J.-M. Fromentin, O. Hoegh-Guldberg, F. Bairlein, Ecological responses to recent climate change, Nature 416 (2002) 389–395.
[46] J. He, G. Christakos, J. Wu, P. Jankowski, A. Langousis, Y. Wang, W. Yin, W. Zhang, Probabilistic logic analysis of the highly heterogeneous spatiotemporal HFRS incidence distribution in Heilongjiang province (China) during 2005-2013, PLoSNegl. Trop. Dis. 13 (2019), e0007091, https://doi.org/10.1371/journal.pntd.0007091.
[47] Z. Hubálek, I. Rudolf, The epidemic process in zoonoses and sapronoses, in: Z. Hubálek, I. Rudolf (Eds.), Microbial Zoonoses and Sapronoses, Springer, Netherlands, Dordrecht, 2011, pp. 33–49, https://doi.org/10.1007/978-90-481-9657-9_5.
[48] R. Rupasinghe, B.B. Chomel, B. Martínez-López, Climate change and zoonoses: a review of the current status, knowledge gaps, and future trends, Acta Trop. 226 (2022), 106225.
[49] M.L. L'Heureux, M.K. Tippett, A.G. Barnston, Characterizing ENSO coupled variability and its impact on North American seasonal precipitation and temperature, J. Clim. 28 (2015) 4231–4245.
[50] C.F. Ropelewski, M.S. Halpert, Global and regional scale precipitation patterns associated with the El Niño/southern oscillation, Mon. Weather Rev. 115 (1987) 1606–1626.
[51] N.Chr Stenseth, G. Ottersen, J.W. Hurrell, A. Mysterud, M. Lima, K. Chan, N. G. Yoccoz, B. Ådlandsvik, Review article. Studying climate effects on ecology through the use of climate indices: the North Atlantic oscillation, El Niño southern oscillation and beyond, Proc. R. Soc. Lond. B Biol. Sci. 270 (2003) 2087–2096.
[52] Y. Sun, Y.H. Wei, Y. Yang, Y. Ma, S.J. de Vlas, H.W. Yao, Y. Huang, M.J. Ma, K. Liu, X.N. Li, X.L. Li, W.H. Zhang, L.Q. Fang, Z.C. Yang, W.C. Cao, Rapid increase of scrub typhus incidence in Guangzhou, southern China, 2006-2014, BMC Infect. Dis. 17 (2017) 13, https://doi.org/10.1186/s12879-016-2153-3.
[53] L.P. Yang, J. Liu, X.J. Wang, W. Ma, C.X. Jia, B.F. Jiang, Effects of meteorological factors on scrub typhus in a temperate region of China, Epidemiol. Infect. 142 (2014) 2217–2226, https://doi.org/10.1017/S0950268813003208.
[54] J.G. Olson, A.L. Bourgeois, Changing risk of scrub typhus in relation to socioeconomic development in the Pescadores islands of Taiwan, Am. J. Epidemiol. 109 (1979) 236–243.
[55] Y.S. Lee, P.H. Wang, S.J. Tseng, C.F. Ko, H.J. Teng, Epidemiology of scrub typhus in eastern Taiwan, 2000–2004, Jpn. J. Infect. Dis. 59 (2006), 235238.